Patterns of Quaternary deformation and rupture propagation associated with an active low-angle normal fault, Laguna Salada, Mexico: Evidence of a rolling hinge?

John M. Fletcher*
Ronald M. Spelz
Departamento de Geología, CICESE, Ensenada, Baja California México C.P. 22860

ABSTRACT

The Laguna Salada rift basin is within the zone of shearing between the Pacific and North American plates and is an asymmetric half-graben controlled on its eastern margin by the Laguna Salada fault and the Cañada David detachment. Both faults dip west, have accommodated >10 km of offset since the middle-late Miocene, and are associated with an extensive late Quaternary fault array. The Laguna Salada fault is a high-angle fault that strikes northwest and has an oblique normal-dextral sense of shear. The Cañada David detachment is a low-angle normal fault with a curvilinear trace that extends ~55–60 km and contains two prominent megamullion antiform-synform pairs. The late Quaternary scarp array that extends along the entire mountain front shows remarkable variations with antiformal and synformal megamullions. In antiformal domains, the scarp array is generally wider, closer to the mountain front (<100 m), and contains numerous antithetic scarps. In synformal domains, it is well removed from the mountain front (3.5–10 km) and contains more synthetic scarps. Integrated deformation across the array shows a systematic decrease in the ratio of horizontal:vertical deformation with distance from the Cañada David detachment, which reflects the mechanism of accommodation of the horizontal component of slip, and/or is the direct result of a master fault with a near-surface antilistric geometry. Patterns of sedimentation as well as gravity and seismic data are consistent with the latter and strongly suggest that the Cañada David detachment takes on a high-angle geometry within 5–10 km of the mountain front. Structural analysis of the scarps and range-bounding fault clearly demonstrates a basinward migration of deformation at a variety of scales along the Cañada David detachment. The largest steps (3.5–10 km) in this migration are made in synformal megamullion domains, where the strong divergence of the scarp array from the trace of the Cañada David detachment results in the abandonment of large segments of the detachment and the transfer of large lozenge-shaped tectonic blocks from the hanging wall to the footwall. The basinward migration of deformation and inferred near-surface antilistric geometry are both defining characteristics of the rolling-hinge model of normal faulting. If this model is applicable, our data indicate that the near-surface antilistric bend of the master fault is tighter and more abrupt than previously envisioned.

INTRODUCTION

Low-angle normal faults remain one of the most controversial and poorly understood classes of geologic structures, despite their widespread presence and dominant role in the accommodation of deformation in extensional orogens throughout the world. Two main issues dominate the present controversy: (1) seismicity that can be unequivocally related to normal slip on low-angle fault planes is rare, and (2) the initiation of normal faults with a low-angle inclination (<30°) cannot be explained in terms of modern principles of rock mechanics. Low-angle normal faults have a greater surface area and are more efficient at accommodating horizontal extension than high-angle normal faults. Wernicke (1995) used these facts to argue that earthquakes related to low-angle normal faults should be much larger in magnitude, but much less frequent than other types of faults. Another hypothesis for the lack of widespread seismicity is that low-angle normal faults might slip aseismically (Jackson, 1987). However, this hypothesis appears to be inconsistent with a growing list of examples of extensive arrays of seismogenic surface ruptures associated with low-angle normal faults (e.g., Axen et al., 1999; Boncio et al., 2000; Cichanski, 2000; Sorel, 2000; Hayman et al., 2003; Taylor et al., 2006; Numelin et al., 2007).

The Andersonian stress configuration for extensional regimes requires low-angle normal faults to have high ratios of normal to shear stress, which is not favorable for generating frictional slip. Axen (1992) showed that it is mechanically feasible to produce seismogenic slip on an existing fault with high normal stress if the fault zone is much weaker than the surrounding rock. Therefore, high pore-fluid pressure and/or a thick zone of phyllosilicate-rich fault gouge are sufficient to produce seismogenic slip on an existing low-angle normal fault in an Andersonian stress regime. However, these mechanical arguments do not explain how a low-angle normal fault would form in the first place. Other workers have proposed that Andersonian stress regimes are overly simplistic, and ignore other factors like topographic loads, lateral density variations, and other sources of horizontal and vertical shear stress that will cause the principal stress axes to rotate from the predicted horizontal and vertical alignment (e.g., Yin, 1989; Wernicke, 1995; Westaway, 1999).

There are essentially three main models for the formation of low-angle normal faults, which we refer to as (1) original low-angle fault model,

*jfletche@cicese.mx

Geosphere; August 2009; v. 5; no. 4; p. 385–407; doi: 10.1130/GES00206.1; 15 figures; 1 table.

(2) domino-block rotation model, and (3) rolling-hinge rotation model. Numerous examples of normal faults that were originally formed in the upper crust with a low-angle orientation have been documented in extensional orogens throughout the world. The documentation of the original low-angle orientation is based on diverse, multidisciplinary data sets that include palinspastic restoration of offset markers with a known original geometry, thermochronologic characterization of footwall cooling histories, and paleomagnetic data (see reviews by Wernicke, 1995; Axen, 2004). However, such faults that are likely to have formed according to the original low-angle fault model raise important questions about inadequacies in our understanding of the geodynamics of extension.

Domino-style rotation of fault blocks is common at all scales in extensional settings and most extended terranes can be characterized by spatially discrete dip domains, where stratigraphic layering has been systematically rotated together with normal faults that accommodate the extensional offsets (e.g., Proffett, 1977; Stewart, 1998; Brady et al., 2000). These crustal-scale blocks likely extend to the base of the seismogenic zone and must overlie a subhorizontal region in the middle crust that accommodates the strain compatibility along the base of the rotating blocks. Depending on the geometry of the base of the blocks, the accommodation region could be a narrow fault zone (brittle and/or ductile), into which the higher angle faults sole listrically. Alternatively, the zone could be much thicker and represent a region where the middle crust flows around indentations and into gaps that form near the corners of the blocks. As the block-bounding faults rotate to lower angles, they become less favorably oriented to accommodate further slip. Collettini and Sibson (2001) proposed that slip on normal faults begins to lock up at dip angles <30°, at which point a new set of high-angle normal faults forms to accommodate continued extension and rotation of the first set of normal faults (Proffett, 1977; Miller et al., 1983). However, Brady et al. (2000) demonstrated that in many cases the younger set of faults does not crosscut, but rather merges with the earlier formed set, which remains active down to dip angles <20°. Therefore, in contrast to the original low-angle fault model, the domino-block rotation model is much more consistent with Mohr-Coulomb rock failure in an Andersonian stress regime.

Another kinematic model that invokes the rotation of initial high-angle faults to progressively lower angles is the rolling-hinge model. In this model, the tectonically unloaded footwall is thought to rebound isostatically to form an antiformal bulge that migrates in the direction of tectonic transport and essentially follows the displacement of the upper plate (e.g., Buck, 1988; Wernicke and Axen, 1988; Lavier et al., 1999). It is generally thought that most active slip takes place on the high-angle fault segment that makes up the leading edge of the antiformal bulge, and, as segments of the master fault pass through the axis of the antiform, they rotate to shallow angles and become progressively abandoned. Most low-angle normal faults with large offset are antiformally warped and have a macroscopic geometry that is consistent with the rolling-hinge model (Wernicke and Axen, 1988). Mesoscopic deformational fabrics with kinematics consistent with the migration of a rolling hinge were first reported by Bartley et al. (1989) and have since been documented in large-magnitude normal fault systems throughout the world (see review by Axen and Bartley, 1997). The rolling-hinge model is consistent with many characteristics of large-magnitude low-angle normal faults as well as with the main theories of rock failure in that the low-angle geometry is achieved by rotation of a preexisting high-angle fault. However, as noted by Axen and Bartley (1997) existing observational data are merely consistent with, but do not demand, the kinematics of the model, and thus a definitive example of a normal fault that has undergone a rolling-hinge evolution has yet to be identified.

Each of the three models for the formation of low-angle normal faults makes specific predictions for the geometry and kinematics of the faults, which can be tested by observational data. In a growing number of recent studies, workers have identified examples of seismically active low-angle normal faults that provide a unique opportunity to test geodynamic models of continental extension. Evidence for seismogenic slip on low-angle normal faults is based on both patterns of seismicity and earthquake source parameters (e.g., Abers, 1991; Rietbrock et al., 1996; Hatzfeld et al., 2000; Abbott et al., 2001; Floyd et al., 2001; Chiaraluce et al., 2006; Little et al., 2006), as well as the presence of extensive Quaternary scarp arrays associated with low-angle normal faults that control well-developed mountain fronts (e.g., Axen et al., 1999; Boncio et al., 2000; Cichanski, 2000; Sorel, 2000; Hayman et al., 2003; Taylor et al., 2006; Numelin et al., 2007).

The Cañada David detachment controls the southern portion of Laguna Salada rift basin in the northern Gulf of California extensional province, and in many ways is ideally suited for addressing the controversial issues surrounding the geodynamic evolution of low-angle normal faults. The fault is a long-lived structure that has accommodated at least 14 km of extensional displacement in the east-northeast direction since the late Miocene, and an extensive array of Quaternary scarps is found along its entire length (~55–60 km). Therefore, this system potentially provides a unique opportunity to characterize both the finite strain accumulated over millions of years as well as the infinitesimal strain associated with the latest earthquake cycles. The Laguna Salada basin is located near the axis of Pacific–North American plate margin shearing and has abundant modern seismicity, which reflects relatively fast rates of tectonism in the area. The seismogenic surface ruptures associated with the Cañada David detachment are recorded by a sequence of eight alluvial fan surfaces that range in age from modern to at least 204 ± 11 ka old, and they are exceptionally well preserved due to the hyperarid microclimate that likely has affected the basin throughout the late Quaternary (Spelz et al., 2008). In summary, the large scale of this detachment fault system combines with relatively fast rates of tectonism and exceptional rupture preservation to form an ideal area for testing geodynamic models of low-angle normal faults.

In this study we present field relationships showing that a major Quaternary scarp array is genetically related to the Cañada David detachment, a hypothesis that was originally proposed by Axen et al. (1999). We document important variations in the magnitude of Quaternary slip as well as the ratio of horizontal:vertical deformation accommodated by surface ruptures located along the Cañada David detachment and use these observations to give new insight into how seismic ruptures propagate to the surface along low-angle normal faults. We demonstrate that the locus of normal faulting has systematically migrated in the direction of tectonic transport along several major segments of the master detachment fault. We then combine the structural analysis of the Quaternary scarp array with gravimetric data, earthquake seismicity, and other independent observational data to help characterize the subsurface geometry of the Cañada David detachment and test evolutionary models for the formation of low-angle normal faults.

REGIONAL GEOLOGY

The Sierras Cucapa and El Mayor are a set of fault-bounded mountain ranges located in the northern Gulf of California extensional province. They are composed predominantly of Mesozoic crystalline basement that has been dismembered from similar terranes found to the northwest in Baja California as well as to the southeast in Sonora. Although the highest peaks are generally only ~1000 m in elevation, the mountains are topographically rugged, which contrasts strongly with the extensive, flat, sub-sea-level sedimentary basins that surround them. The abundant seismic activity in this region confirms that it is located near the middle of the zone of shearing between the North American and Pacific plates (Fig. 1).

Both Sierra El Mayor and Sierra Cucapa are internally cut by an intense array of low- and high-angle faults that generally accommodate deformation with an instantaneous principal extension axis oriented west-southwest–east-northeast (Axen and Fletcher, 1998a; Axen et al., 1999; Chora-Salvador, 2003). Although most of the seismicity and plate-margin shearing is located to the east of Sierras El Mayor and Cucapa, the main active range-front faults are along the western margin, where they form the abrupt structural boundary between the uplifted mountains and the sub-sea-level Laguna Salada basin (Fig. 1).

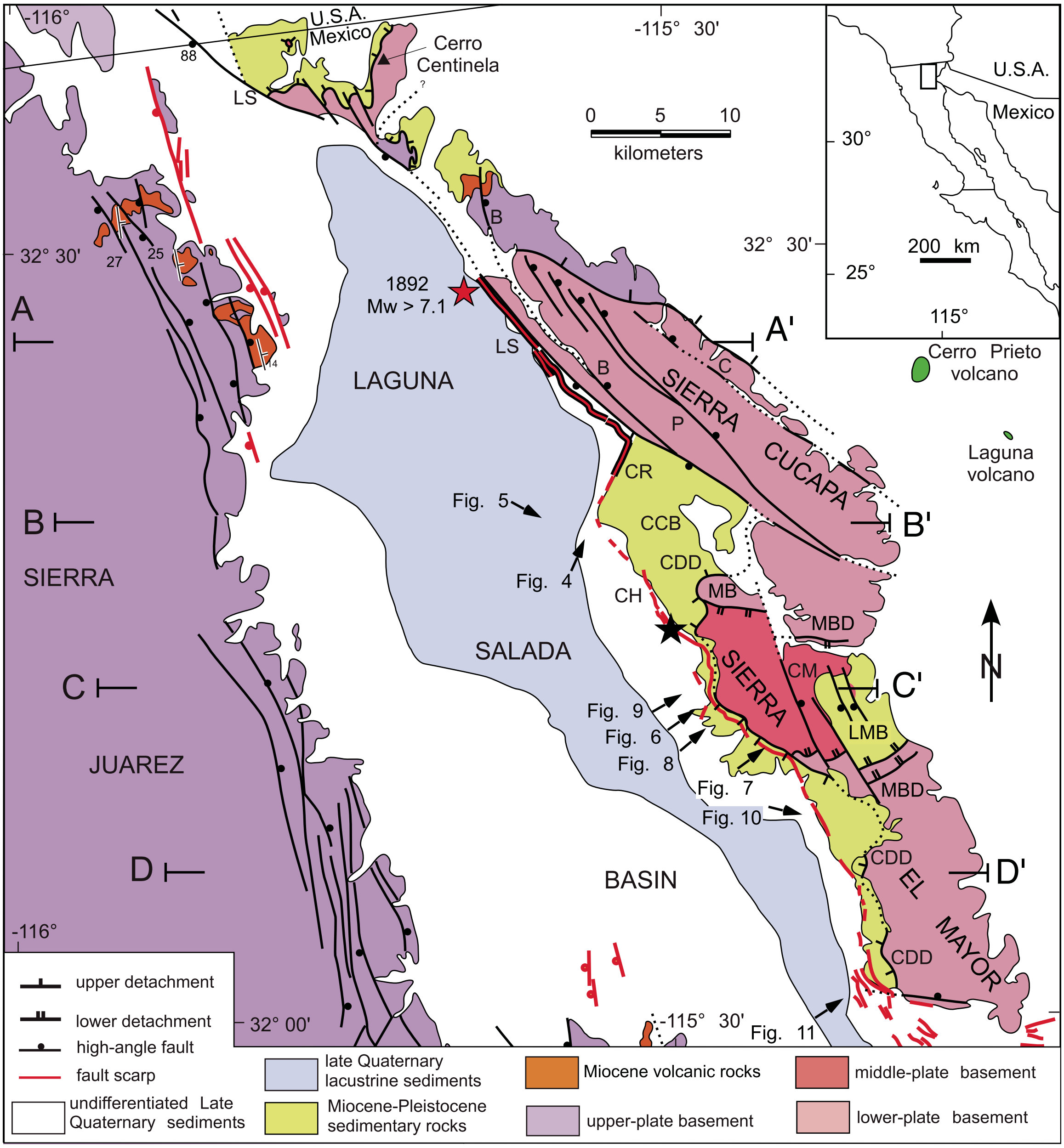

Figure 1. Schematic geologic map of the Laguna Salada basin, which is a half-graben controlled by the Laguna Salada and Cañada David faults along its eastern margin. Arrows show the approximate orientation and location of field photographs shown in subsequent figures. Stars denote possible locations of major epicenters, as discussed in the text. The locations for the four serial cross sections (A-A', B-B', C-C', and D-D') correspond to those shown in Figure 15. Abbreviations: LSF—Laguna Salada fault, B—Borrego fault, P—Pescadores fault, C—Cucapa fault, CR—Cañón Rojo fault, CH—Chupamirtos fault, CCB—Cerro Colorado basin, CDD—Cañada David detachment, MB—Monte Blanco dome, MBD—Monte Blanco detachment, CM—Central Mayor fault. LMB—Lopez Mateos Basin; LS—Laguna Salada fault. Green map unit denotes Quaternary volcanoes located on the plate margin.

The western margin of Sierra El Mayor, where substantial tectonic activity is concentrated, is controlled by the west-dipping Cañada David detachment. This structure was first documented by Siem and Gastil (1994), and later Axen and Fletcher (1998) showed that it could be traced for ~45 km along the entire western margin of Sierra El Mayor. The Cañada David detachment is a west-dipping low-angle normal fault that juxtaposes a Miocene–Pleistocene synrift sedimentary sequence against Mesozoic crystalline basement (Siem and Gastil, 1994; Axen and Fletcher, 1998a; Dorsey and Martín-Barajas, 1999; Martín-Barajas et al., 2001). The fault zone commonly dips 10°–20° and has 1–2 m of varicolored clay gouge surrounded by a zone of cataclasite that ranges to 100–200 m in thickness. Activity along the Cañada David detachment is believed to have begun ca. 12 Ma ago and has accommodated 5–7 km of vertical uplift, as indicated by low-temperature thermochronology of footwall rocks (Axen et al., 2000). To the north, the Cañada David detachment ends against the northwest-striking Laguna Salada fault, which is a subvertical normal-dextral fault that controls the western margin of the Sierra Cucapa. To the south, the Cañada David detachment and its uplifted footwall abruptly disappear along a margin of sedimentary basin fill, a transition that must be structurally controlled by yet-undocumented faults in the subsurface. Like most large-offset normal faults, the Cañada David detachment is corrugated and shows a strongly curvilinear trace with two major antiform-synform megamullion pairs. In this study we show that the megamullion corrugations play a dominant role in the distribution and character of adjacent fault scarps.

An extensive scarp array is found along the entire length of the mountain front controlled by the Cañada David detachment. However, most of the scarps do not coincide with the exact trace of the Cañada David detachment, but rather form a complex array that cuts a sequence of eight late Quaternary alluvial fan surfaces that have been mapped along the flank of the western Sierra El Mayor mountain front. The fan surfaces are referred to in reverse chronologic order, Q_1 being modern alluvial deposits and Q_8 forming the oldest surfaces (Spelz et al., 2008). In some cases the scarp array is found as much as 10 km west of exposures of the Cañada David detachment. Based on detailed mapping and topographic profiles from an ~9 km segment of the scarp array, Axen et al. (1999) first argued that these fault scarps represent surface ruptures related to Quaternary slip on the range-bounding Cañada David detachment. This was based primarily on three important observations. (1) The scarp-forming faults showed abrupt changes in orientation and followed the curvilinear trace of the Cañada David detachment. (2) The scarps form broad arrays with as many as 15 or more scarps in transects perpendicular to the range front, which is consistent with the system of scarp-forming faults that emanate from a master detachment just below the surface. (3) The scarp arrays contain numerous antithetic (basin-side up) faults and total slip has high heave:throw ratios, which also is consistent with surface deformation controlled by seismogenic slip on a low-angle normal fault. Although we continue to agree with the basic conclusion of a genetic relationship between the Cañada David detachment and the surface ruptures, our study shows that none of these three main characteristics can characterize all segments of the scarp array. In fact, it is precisely the wide variations in the character of the fault system that gives new insight into not only how to recognize active low-angle normal faults, but also to understand how range-bounding detachments evolve during progressive deformation.

TOPOGRAPHIC PROFILES ACROSS SCARP-FORMING FAULTS

During the past ten years alluvial fan surfaces and fault scarps have been mapped in the hanging wall of the Cañada David detachment along the western margin of the Sierras El Mayor and Cucapa at a scale of 1:6000. In addition, 12 topographic profiles across the fault-scarp arrays were measured in key locations (Fig. 2). Profile sites were chosen on the basis of three main criteria: (1) complete exposure of the full width of the scarp array, (2) offset fan surfaces that can be confidently correlated across scarps with minimal modification by later erosion and/or deposition, and (3) structural context. Regarding the last criterion, we attempted to characterize all important along-strike variations that could be related to changes in the geometry and kinematics of either the scarp array or the adjacent range-bounding fault. Topographic transects were surveyed in a direction subperpendicular to the strike of the scarp-forming faults (Fig. 2). Most commonly, the profiles have an east-northeast azimuth that is subparallel to the inferred direction of tectonic transport of the Cañada David detachment. Portions of the scarp array with evidence for oblique-slip kinematics were not included in this study. Surveying was performed with a laser distance meter total station that has centimeter-scale accuracy, which was more than sufficient for measuring offset of the terrace deposits composed of unconsolidated boulder conglomerate.

Palinspastic restoration of individual transects was preformed to characterize the total deformation across the scarp array, which commonly includes both synthetic (those that are west facing and upthrown on the range side of the scarp) and antithetic (those that are east facing and upthrown on the basin side of the scarp). In order to systematically perform the palinspastic restoration, we assume that all scarp-forming faults dip 65°, which is the average orientation of scarp-forming faults measured in this study and by Axen et al. (1999) in Laguna Salada. In addition to the total slip, we also report the net horizontal and net vertical slip components recorded in each transect across the scarp array. If the scarps had originated from a single master fault at depth and deformation was conserved between the scarps and the master fault, then the dip of the master fault should have controlled the ratio of vertical:horizontal net slip components. In the case of normal faults, one would expect a greater number of antithetic ruptures to be associated with slip on more shallowly dipping master faults, because antithetic scarps add to the net horizontal slip component but subtract from the net vertical slip component. A more intuitive way of visualizing the ratio of vertical:horizontal net slip components is to express it as the dip of a hypothetical master fault, which is simply calculated by taking the arctangent of the ratio of vertical:horizontal net slip components. It is important to emphasize that the hypothetical master-fault dip calculated in this manner is simply a structural parameter used to visualize the relative proportion of net slip across synthetic and antithetic scarps at different locations in the scarp array. We offer several alternative hypotheses to explain the observed variations in the hypothetical master-fault dip.

Table 1 summarizes the main characteristics of the fault-scarp arrays, which show marked variations in width, morphological expression, total number of scarps and proportion of synthetic versus antithetic scarps. The main variations occur between four main segments that coincide well with the large-scale megamullion corrugations of the Cañada David detachment (Fig. 2). Representative topographic profiles from each domain are shown in Figure 3.

Northern Synform Domain

The northernmost segment of the Cañada David detachment forms a major synformal corrugation and ends abruptly against the Laguna Salada fault (Figs. 1 and 2). Scarp-forming faults in this domain occur well west of the detachment and along discrete high-angle normal faults that flank the Laguna Salada basin. The northernmost fault is called the Cañón Rojo fault and, just like the Cañada David detachment, it abruptly ends against the Laguna Salada fault.

Cañón Rojo Fault

Scarps related to the total slip history of the Cañón Rojo fault, from middle Quaternary to recent time, are not preserved, and only the scarps of the most recent event, the M_w >7.1 earthquake in 1892, are found along the trace of the Cañón Rojo fault (Mueller and Rockwell, 1995). During this event, ground rupture propagated southeastward along a segment of the northwest-striking Laguna Salada fault (Mueller and Rockwell, 1995), but did not continue all the way to the existing Cañada David detachment. Beyond the intersection with the Cañón Rojo fault, the Laguna Salada fault extends for another ~17 km to the southeast. Although hydrothermal activity is present along this southeastern segment (Barnard, 1968), no Quaternary scarps were observed, and the Laguna

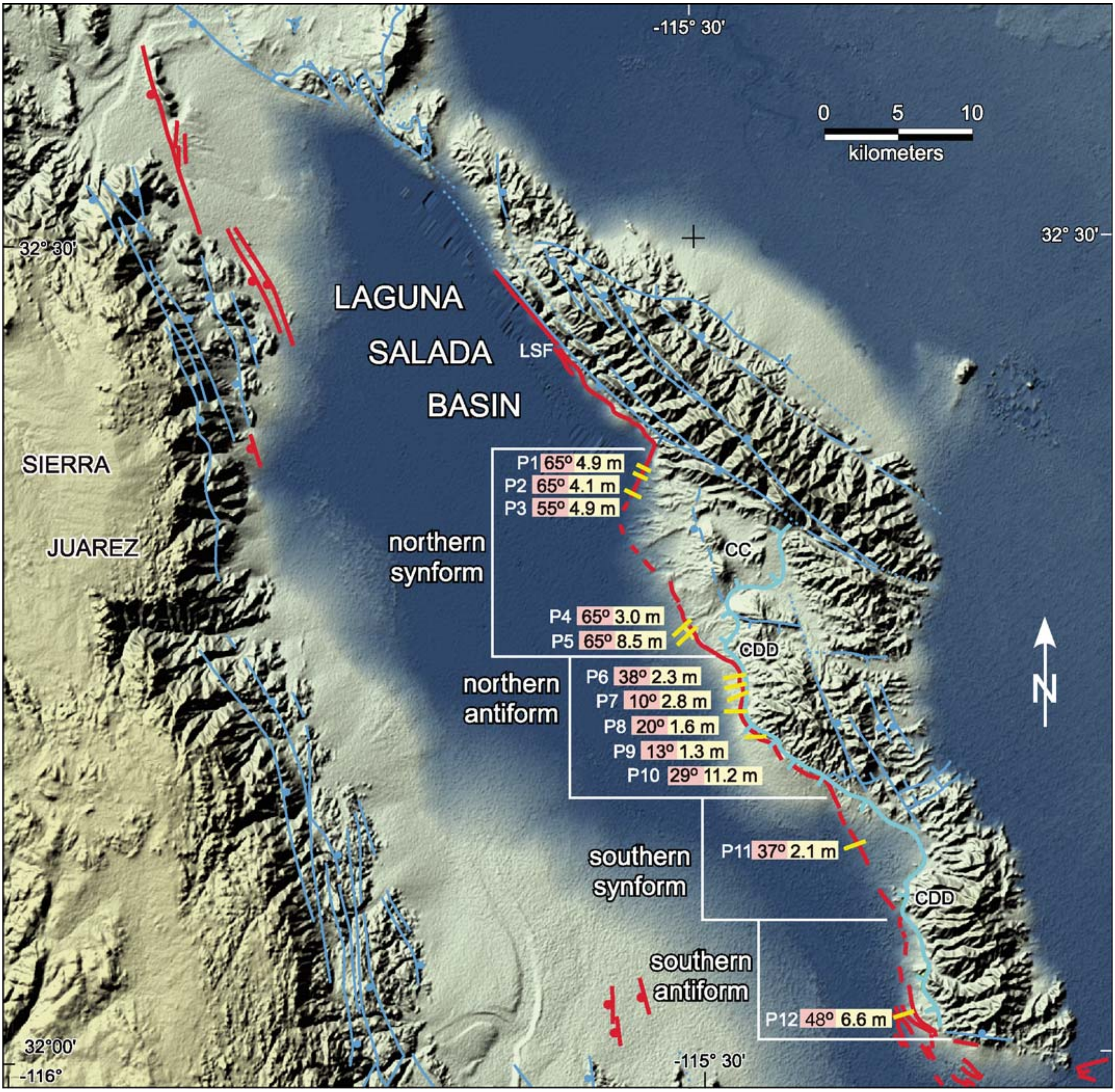

Figure 2. Shaded relief map of the Laguna Salada basin showing distribution of faults (blue), Quaternary scarps (red), and topographic profiles (P1–P12, yellow) used to measure net displacement across the fault scarps. Each profile label contains name, net displacement, and hypothetical master-fault dip. The Cañada David detachment (CDD, light blue) is subdivided into four main segments based on megamullion corrugations. The northern and southern limits of the domains are delimited by straight horizontal lines. Digital elevation model (DEM) data were compiled from Shuttle Radar Topography Mission (SRTM) and GEoModelos de Elevación (GEMA) data sets. CC—Cerro Colorado; LSF—Laguna Salada fault.

TABLE 1. SEISMOGENIC SLIP ESTIMATED FROM TOPOGRAPHIC PROFILES ACROSS THE QUATERNARY SCARP ARRAY OF THE EASTERN MARGIN OF LAGUNA SALADA

Location, profile	Location		Distance to CDD (km)†	Array width (m)	Number of scarps§	Relative scarp age#	Strike of scarps	Profile Azimuth (°)	Horizontal net slip (Σh_i in m)	Vertical net slip (Σv_i in m)	Total net slip (m)**	$\frac{\Sigma h_i}{\Sigma v_i}$	Hypothetical master-fault dip (°)††
	Easting*	Northing*											
Northern synform domain													
Profile 1	637909	3581117	10.404	40	3S:0A	Q1–Q2	2	91.5	2.1	4.4	4.9	0.5	65
Profile 2	637721	3580670	10.396	30	2S:0A	Q1–Q2	10	100	1.7	3.7	4.1	0.5	65
Profile 3	637221	3579603	10.518	230	12S:4A	Q3–Q4	11	101	2.8	4.0	4.9	0.7	55
Profile 4	640736	3570127	2.885	25	1S:0A	Q4–Q5	316	46	1.3	2.7	3.0	0.5	65
Profile 5	640970	3569795	2.571	55	2S:0A	Q4–Q5	316	46	3.6	7.7	8.5	0.5	65
Average			7.355										63
Northern antiform domain													
Profile 6	644438	3566787	0.043	40	1S:2A	Q3–Q4	348	78	1.8	1.4	2.3	1.3	38
Profile 7	644492	3566702	0.014	50	3S:2A	Q3–Q4	347	77	2.8	0.5	2.8	5.8	10
Profile 8	644705	3566368	0.004	30	1S:1A	Q3–Q4	334	64	1.5	0.6	1.6	2.7	20
Profile 9	644687	3566289	0.022	25	1S:1A	Q3–Q4	11	101	1.2	0.3	1.3	4.2	13
Profile 10§§	645076	3563659	0.100	305	8S:7A	Q3–Q4	3	93	9.7	5.5	11.2	1.8	29
Average			0.037										22
Southern synform domain													
Profile 11	652154	3556345	4.259	260	2S:3A	Q3–Q4	340	70	1.7	1.3	2.1	1.3	37
Southern antiform domain													
Profile 12	655548	3544281	1.659	517	7S:4A	Q6–Q7	342	72	4.4	4.8	6.6	0.9	48

*Universal Transverse Mercator (NAD-27 Mexico).

†The distance was measured from the easternmost scarp in the array to the trace of the detachment fault. CCD is Cañada David detachment.

§Total number of scarps across the profile is expressed in terms of the number of synthetic scarps versus antithetic scarps (#S:#A).

#Relative scarp age is based upon the oldest unit not cut and the youngest unit cut by the scarp-forming faults.

**Total net slip $= \sqrt{(\Sigma h_i)^2 + (\Sigma v_i)^2}$

††Hypothetical master-fault dip $= \tan^{-1}\left[\Sigma v_i / \Sigma h_i\right]$

§§Profile compiled from Axen et al. (1999).

Salada fault defines a relict mountain front southeast of its intersection with the Cañón Rojo fault (Fig. 4).

Fault scarps along the trace of the Cañón Rojo fault are found ~10 km northwest of the Cañada David detachment, which is the greatest distance observed between the traces of the Cañada David detachment and the scarp array (Table 1). The scarps typically display free faces and cut deposits as young as Q_2 with an average vertical offset of 2–4 m, which is consistent with their formation during the M_w ~7.1 earthquake in 1892, as proposed by Mueller and Rockwell (1995; Fig. 2). The scarp array along the Cañón Rojo fault is dominated by synthetic (range-side up) fault scarps. Near the intersection with the Laguna Salada fault, it is characterized by a single synthetic scarp that defines the trace of the fault (Fig. 4). Approximately 1.5 km south of the intersection, scarps begin to splay from the main fault trace and form an array of multiple scarps. Profile 2 shows a representative topographic profile of this segment where the array is ~43 m wide and composed of two synthetic fault scarps that cut Q_3 (Fig. 3). Because the scarps are predominantly synthetic, the hypothetical master-fault dip is equal to the assumed dip of the scarp-forming faults (i.e., 65°), and the relative proportion of horizontal to vertical deformation is only 0.5 (Table 1). This multiple synthetic fault-scarp array can be traced for at least another kilometer to the south until the Cañón Rojo fault ends in a diffuse manner as the branching pattern gains complexity. Near its southern termination the array consists of 16 individual scarps that cover a much broader zone (Table 1, profile 3). Another anomalous characteristic of profile 3 is the presence of four small antithetic scarps, the only antithetic scarps observed in the entire northern synformal domain. Regardless of the width or number of scarps in any given transect, total slip related to the 1892 event (~5 m) does not vary significantly along the length of the Cañón Rojo fault (Table 1, profiles 1–3).

South of the termination of the 1892 rupture, the new mountain front that has been established along the Cañón Rojo fault continues to be defined by uplifted basin fill deposits, but almost all late Quaternary scarps have been erased by erosion. Toward the south the topographic uplift across the fault decreases, as observed by a decrease in the relative height of dissected alluvial fan surfaces in the footwall.

Chupamirtos Fault

In the southern portion of the northern synformal domain, the new mountain front bends to the southeast; Barnard (1968) named the fault that corresponds to this segment the Chupamirtos fault to distinguish it from the northeast-striking Cañón Rojo fault. Like the Cañón Rojo fault, the Chupamirtos fault shows predominantly dip-slip striae, and thus its principal instantaneous extension direction is east-northeast, similar to the Cañada David detachment. The Chupamirtos fault scarp array is typically narrow (~70 m) and consists exclusively of synthetic scarp-forming faults (profiles 4 and 5; Table 1; Fig. 2). Profile 5 is located ~2.6 km west from the range-front fault and consists of two synthetic fault scarps cutting Q_5 (Fig. 3). Maximum vertical offset of the highest scarp is 7.23 m; however, similar Q_5 deposits closer to the range-front fault (~0.5 km) show ~4 times less vertical separation, which suggests either multiple slip events associated with the higher scarps and/or a strong decreasing slip gradient toward the southeast. The ratio of horizontal to vertical components of shear across this composite scarp array yields a hypothetical master-fault dip of 65°, as expected for an array composed exclusively of synthetic scarps (Table 1).

Leeds (1979) proposed that the epicenter of a M_L 6.5 earthquake on 30 December 1934 was located near this fault (Fig. 1). The earthquake focal mechanism determined by Doser (1994)

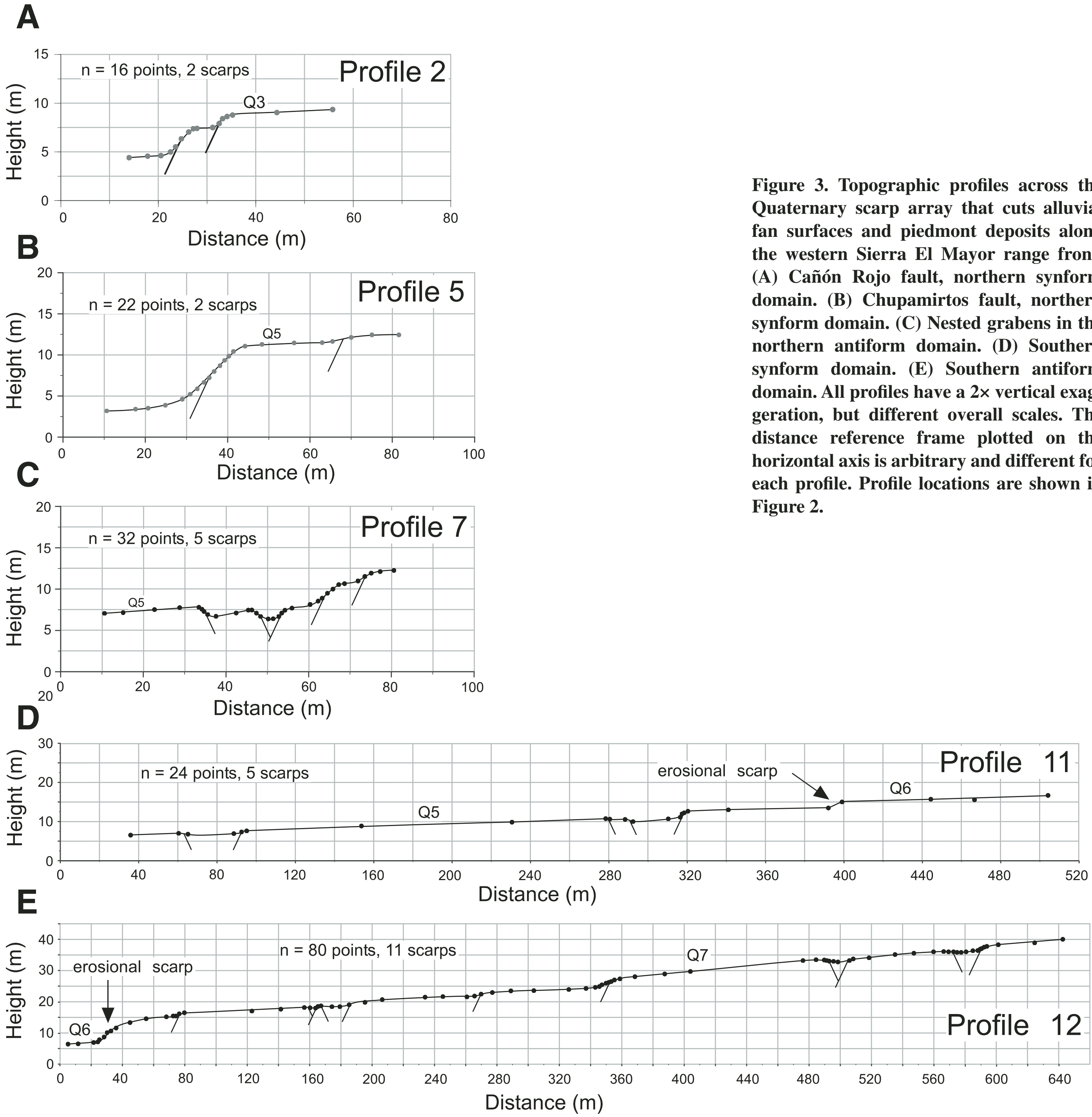

Figure 3. Topographic profiles across the Quaternary scarp array that cuts alluvial fan surfaces and piedmont deposits along the western Sierra El Mayor range front. (A) Cañón Rojo fault, northern synform domain. (B) Chupamirtos fault, northern synform domain. (C) Nested grabens in the northern antiform domain. (D) Southern synform domain. (E) Southern antiform domain. All profiles have a 2× vertical exaggeration, but different overall scales. The distance reference frame plotted on the horizontal axis is arbitrary and different for each profile. Profile locations are shown in Figure 2.

for this event indicates nearly pure right-lateral slip on a northwest-striking plane. Although the strike of the Chupamirtos fault is consistent with the focal mechanism, the dip-slip striae are not. In places, scarps along the Chupamirtos fault cut Q_3 Holocene(?) alluvial fan surfaces, but they contain no free faces and, in general, are more degraded (scarps of similar heights have shallower slopes) than those observed along the Cañón Rojo fault. Therefore, it is possible that the 1934 event either did not produce a surface rupture, or it was not associated with the Chupamirtos fault.

In the southern part of the northern synformal domain, the Chupamirtos scarp array projects obliquely toward the Sierra El Mayor range front and, at the range-front intersection, it makes a 55° angle with the Cañada David detachment (Fig. 1). However, detailed mapping in the region shows that the younger Chupamirtos fault does not crosscut either the Cañada David detachment or lithologic markers in its footwall. Moreover, although late Quaternary scarps are absent along the Cañada David detachment to the north of this intersection, they are ubiquitous to the south (Figs. 1 and 5). This is clear evidence that the Chupamirtos fault separates inactive and active segments of the Cañada David detachment and is thus a good example of a high-angle fault that is genetically related to and is in the hanging wall of a low-angle master fault. It is important to emphasize that beyond the change in orientation that occurs around a broad curve in the new mountain front, there is no other fundamental difference between the Chupamirtos fault and the Cañón Rojo fault.

Throughout the northern synform domain the Cañada David detachment projects under the Cerro Colorado basin toward the Cañón Rojo and Chupamirrtos faults. The crosscutting relationships observed at the surface imply that these clearly younger faults do not crosscut the Cañada David detachment at depth. Instead, it is likely that they simply merge with the older structure, and their intersection defines the limit

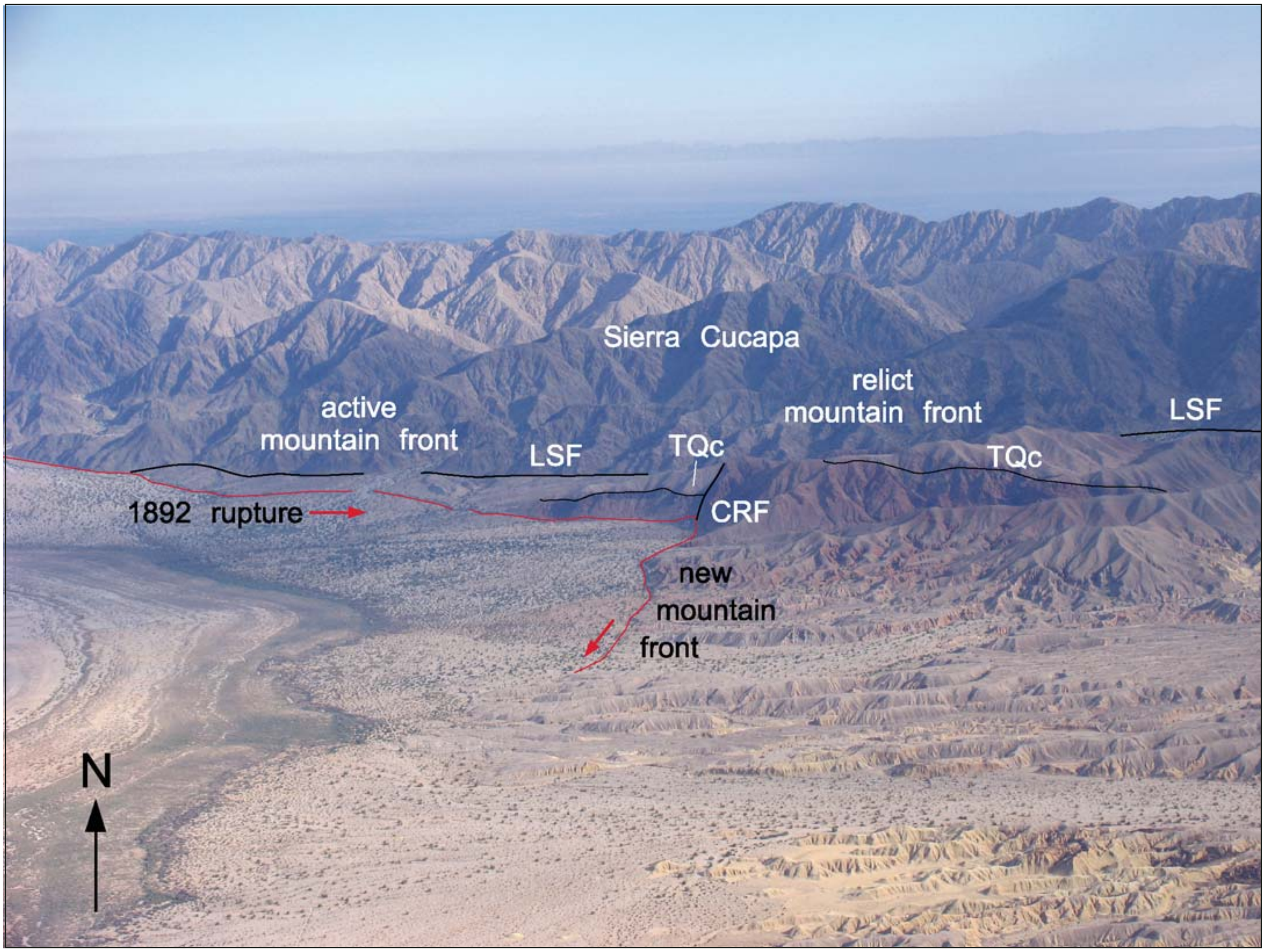

Figure 4. Oblique aerial photograph of the southern Sierra Cucapa showing the intersection between the Laguna Salada fault (LSF) and the Cañón Rojo fault (CRF). The 1892 rupture propagated toward the southeast along the LSF and then abruptly turned into the basin to follow the CRF. Propagation direction is shown by red arrows. The CRF separates active and inactive segments of the LSF and defines the new mountain front along which older basin fill deposits are being uplifted. The yellowish deposit in the foreground is the late Miocene Imperial Formation. The basal contact of the Pliocene–Pleistocene unconsolidated gray gravel (TQc) is offset ~100 m across the CRF. Azimuth of photo is ~035°. The strike lengths of the LSF and the 1892 rupture visible in this photo are ~6.3 and ~5.8 km, respectively. The approximate location and orientation of the photograph are shown in Figure 1.

between active and inactive segments of the Cañada David detachment.

Crosscutting relationships in the northern synform domain clearly show that the locus of normal faulting has migrated westward by as much as ~12 km in the direction of tectonic transport of the basin-bounding fault system. A major segment of the Cañada David detachment that accommodated normal faulting throughout most of the Neogene (Axen et al., 2000) has been abandoned. A new mountain front is becoming established where basin fill is being uplifted in the footwall of the Cañón Rojo and Chupamirtos faults, which record multiple seismic events (Figs. 1, 4, and 5). The oldest and most dissected alluvial fan surfaces (Q_7) found in the footwall of these two faults are correlated with fan surfaces that yield terrestrial cosmogenic nuclide exposure ages of 204 ka old, as reported by Spelz et al. (2008). Therefore, the most recent westward migration of deformation predates these fan surfaces.

Located between the abandoned trace of the Cañada David detachment and the new mountain front defined by the Cañón Rojo and Chupamirtos faults is a fault-bounded ridge of basin fill strata named Cerro Colorado (Fig. 2). Cerro Colorado is flanked by steep Q_6 and Q_7 alluvial fan surfaces, which are not cut by faults along the base of the ridge. Therefore, we interpret the westward migration of normal faulting in the northern synform domain to have occurred in at least two major phases. The first phase produced a new mountain front along the western margin of Cerro Colorado. These faults were abandoned after the formation of Q_7 alluvial fan surfaces (204 ka ago; Spelz et al., 2008), when normal faulting became established along the active Cañón Rojo and Chupamirtos faults.

Northern Antiform Domain

The northern antiform domain is marked by the obvious westward bulge of northern Sierra El Mayor (Figs. 1 and 2). A prominent feature along its northern limit is the Monte Blanco dome, which is an antiformal deflection of the Cañada David detachment that is remarkably similar to the turtlebacks found in Death Valley (e.g., Miller and Pavlis, 2005; Fig. 5 herein). The Cañada David detachment bends strongly

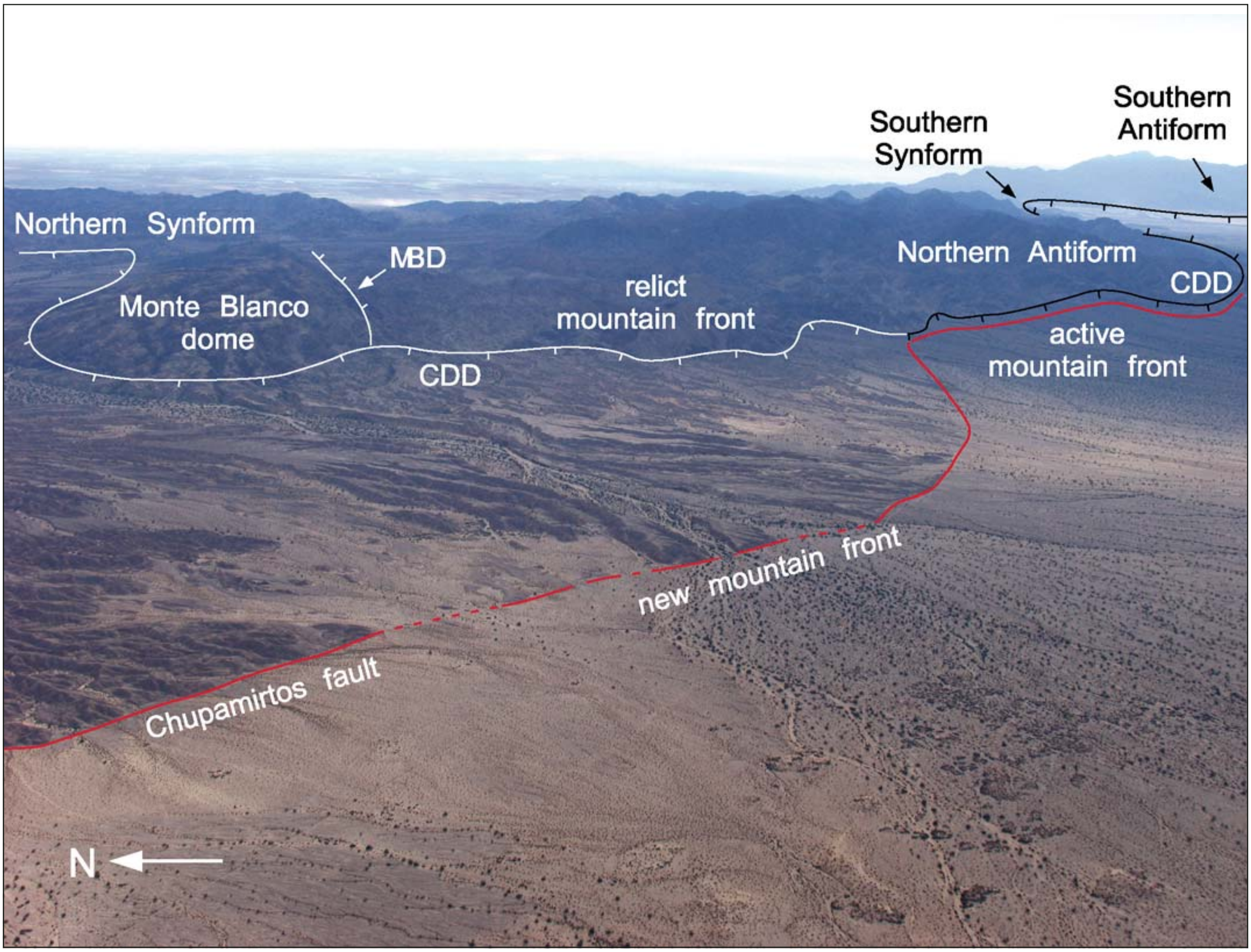

Figure 5. Oblique aerial photograph of the Chupamirtos fault and Cañada David detachment (CDD). The Chupamirtos fault merges with the CDD in the northern antiformal domain just south of the Monte Blanco Dome. MBD—Monte Blanco detachment. A new mountain front is being established along the Chupamirtos fault, and its intersection with the CDD separates active (black) and inactive segments (white) of the CDD. The strike length of the Chupamirtos fault and late Quaternary scarp array in this photo is ~11.4 km. The approximate location and orientation of the photograph is shown in Figure 1.

around the northern side of the dome, whereas the southern side of the dome is bounded by a structurally lower detachment, called the Monte Blanco detachment, that dips to the south and merges westward with the Cañada David detachment (Fig. 1; Axen and Fletcher, 1998b).

The intersection of the Chupamirtos fault with the Cañada David detachment occurs ~3 km south of Monte Blanco dome, and here the scarp array completely changes character. Instead of following relatively straight high-angle faults in the basin, the scarp array occurs very close (4–100 m) to the long-lived Sierra El Mayor mountain front (Fig. 6). The youngest Quaternary unit cut by the scarps in this area is Q_4, which is widely exposed in this domain (Figs. 7 and 8). In some rather remarkable cases, seismogenic ruptures are observed connecting segments of the Cañada David detachment exposed in isolated erosional remnants that emerge from the fan surface (Fig. 7). Although rare, relationships such as these provide the strongest evidence that seismogenic ruptures propagate to the surface along low-angle normal faults.

The Cañada David detachment is curviplanar with a highly curvilinear trace and, as observed by Axen et al. (1999), the scarp array in the northern antiform domain undergoes extreme variations in strike and closely follows the smaller scale megamullion deflections of the Cañada David detachment (Fig. 8). Farther from the mountain front, individual scarps also contain strongly curvilinear traces and change strike by as much as 60° over distances of <200 m (Fig. 9) We argue below that these radical changes in the strike of scarps are to be expected when a seismic rupture propagates toward the surface along an irregular low-angle master fault at depth.

Perhaps the most distinguishing characteristic of the scarp array in this domain is the marked increase in the number of antithetic (basin-side up) scarps, and the array can be thought of as a series of well-defined nested horsts and grabens (Fig. 3, profile 7). Although the antithetic scarps are generally smaller than the synthetic scarps, they typically make up half of the scarps observed in cross-strike transects (Table 1). The array in profile 7 is ~50 m wide and consists of 3 synthetic and 2 antithetic

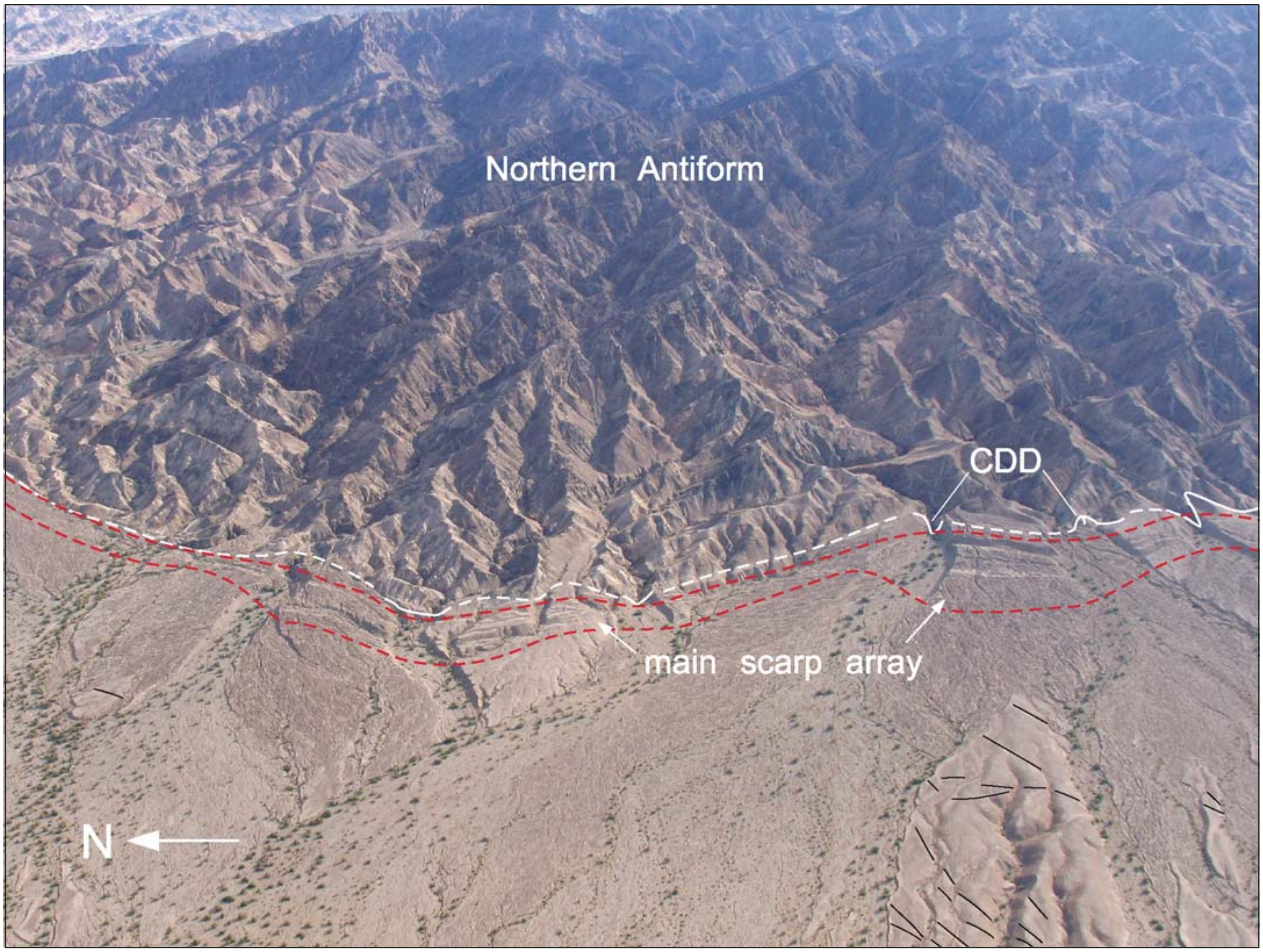

Figure 6. Oblique aerial photograph of the northern antiformal domain showing the strong spatial coincidence of the scarp array and the trace of the Cañada David detachment (CDD). Trace of the Cañada David detachment is shown in white and the approximate limits of a late Quaternary scarp array are shown with the red dashed line. Older scarps can be observed west of the mountain front in the lower right portion of the photograph. The strike length of the main scarp array in this photo is ~2.1 km. The approximate location and orientation of the photograph are shown in Figure 1.

scarps that are found only a few tens of meters away from the trace of the range-front fault (Fig. 3). The integrated deformation across all faults has a net heave of 2.8 m and net throw of 0.5, resulting in a heave:throw ratio of 5.8. The reconstruction thus gives a hypothetical master-fault dip of 10°, which is the shallowest solution in this study. Nearly all the profiles in this domain record high heave-throw ratios and hypothetical master-fault dips that are similar to the measured dip of the Cañada David detachment (Table 1).

The southern limb of the northern antiform, which was the study area of Axen et al. (1999), contains key structural relationships that differ slightly from the northern limb, where most of the new profiles were measured. The southern flank of the northern antiform is composed of alternating north- and northwest-striking segments that define small-scale corrugations of the Cañada David detachment. The northwest-striking segments are commonly defined by simple arrays of 1–3 scarps, whereas the more northward-striking segments become wider and much more complex. We agree with Axen et al. (1999) that this structural pattern likely arises because the north-striking segments are more orthogonal to the overall slip direction across the Cañada David detachment. The profile published by Axen et al. (1999) is a good example of the radical increase in array width (305 m) and number of scarps (15) that is observed in northward-striking segments of the southern flank (Table 1). The total net slip of 11.2 m is much higher than that observed in the other profiles farther north (Table 1) and represents a maximum for the entire domain, as deformation also decreases to the southeast (Axen et al., 1999).

Southern Synform Domain

Upon approaching the southern synformal domain, the scarp array begins another dramatic divergence from the trace of the Cañada David detachment, which follows a geomorphologically more subdued segment of the mountain front (Figs. 1 and 2). Although the Cañada David detachment is not exposed throughout the entire domain, its trace is well defined by a series of outlying hills composed of locally derived conglomerate that is correlative with the

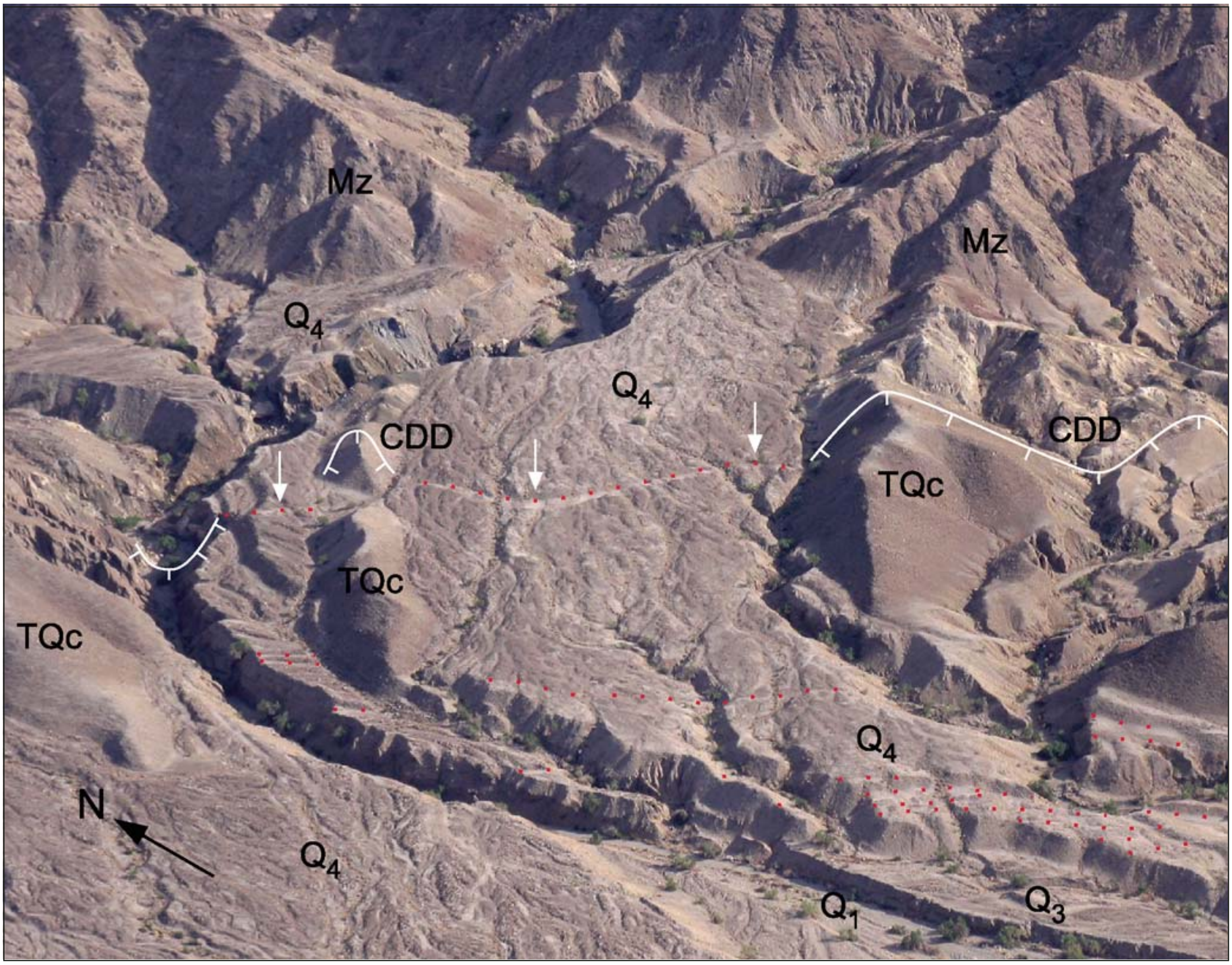

Figure 7. Oblique aerial photograph showing trace of Quaternary scarps (red dotted lines) and the Cañada David detachment (white lines). Note how some Quaternary scarps (white arrows) connect isolated exposures of the Cañada David detachment, which indicates that seismic rupture has propagated to the surface trace of the Cañada David detachment (CDD). TQc—Pliocene–Pleistocene conglomerate; Mz—Mesozoic crystalline basement. Q_1–Q_4 correspond to relative ages of alluvial surfaces; Q_4 is the oldest. Lower edge of photograph is ~250 m long. The approximate location and orientation of the photograph are shown in Figure 1.

Pliocene–Pleistocene conglomerates observed to the north (Fig. 10). In all other domains this unit is found in fault contact with the Mesozoic basement across the Cañada David detachment. At its maximum separation, the scarp array is ~4.5 km from the inferred trace of the Cañada David detachment. As was observed in the northern synform domain, the detachment fault in this domain defines a relict mountain front and deformation has migrated well west of the trace of the Cañada David detachment.

Scarps in the southern synform domain are remarkably straight, and the azimuth of most scarps varies by only 5° from the domain average of 335°, which is subperpendicular to the principle instantaneous extension direction of the Cañada David detachment. However, in contrast to the northern synform domain, the scarp array is much wider (~300 m), and antithetic scarps make an important contribution to the overall deformation, which has a total net slip of 2.1 m and a hypothetical master-fault dip of 37° (Table 1, profile 11). The oldest unit not cut by the array is Q_4. Although Holocene alluvial fan surfaces are not well exposed in this domain, the scarp profiles are significantly more degraded than those to the north (Fig. 3, profile 11). There is a conspicuous absence of scarps over a distance of 2.5 km in the southern portion of this domain and a prominent Q_6 surface is not faulted along the southward projection of the array. However, scarps reappear as the scarp array merges again with the mountain front to the south.

Southern Antiform Domain

The most complete exposure of the scarp array in the southern antiform domain is found in its southern extreme, where alluvial fan surfaces and geomorphic surfaces are very well preserved, and residual hills of older basin fill commonly rise above the alluvial fan surfaces (Fig. 11). Four distinct sets of faults and scarps can be documented in a transect from the mountain front to the basin. (1) Near the mountain front, isolated high standing ridges of Pliocene–Pleistocene gray gravels are found

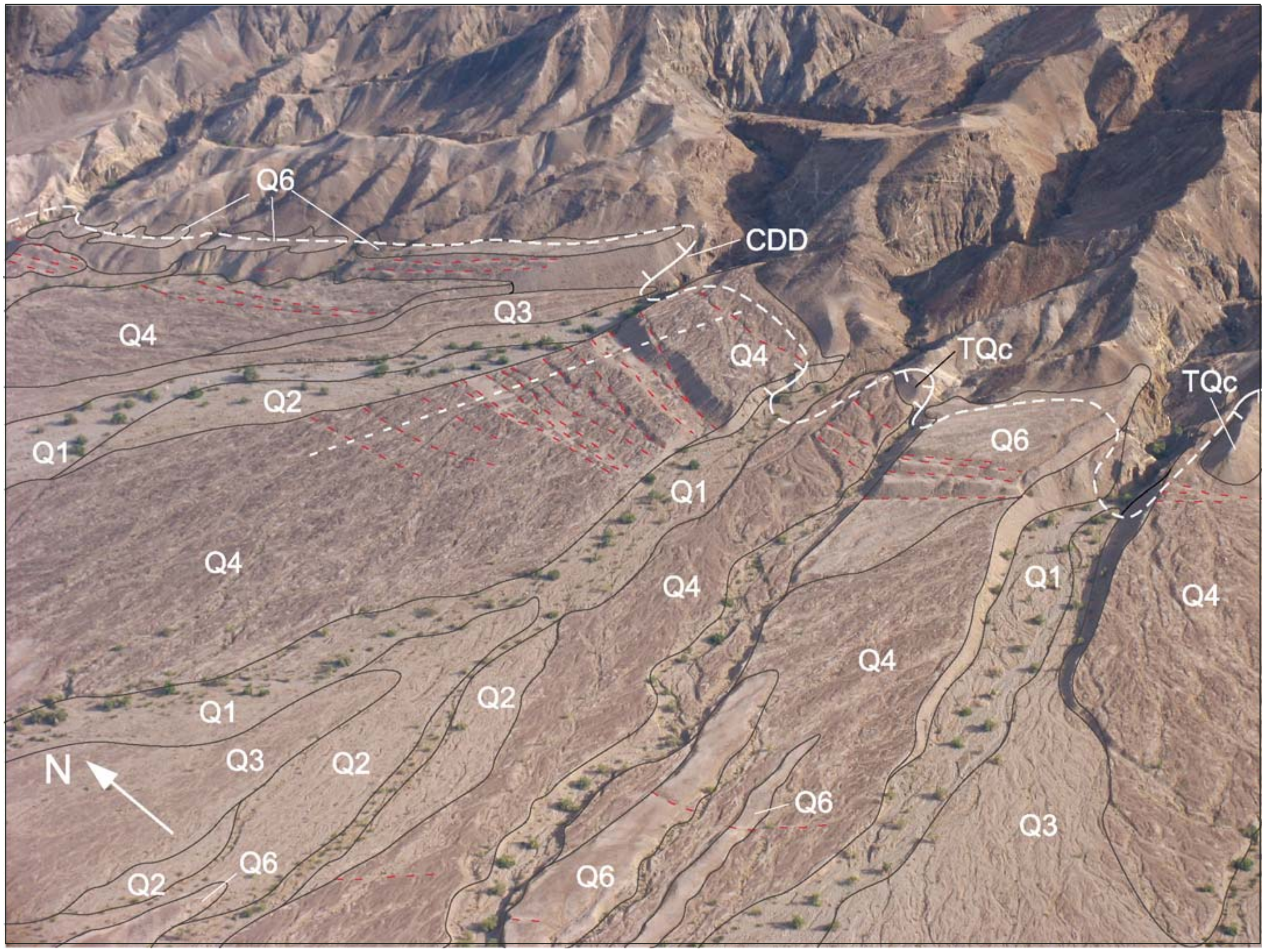

Figure 8. Oblique aerial photograph showing the abundance of antithetic scarps in the scarp array of the northern antiform domain. Note the marked change in orientation of the scarp array around small-scale megamullions in the Cañada David detachment (CDD). Trace of the CDD is shown in white, scarps are shown with thin red dashed lines, and terrace contacts are shown with thin gray lines. The trace of topographic profile 10 is shown by a straight dashed white line, which is 305 m. TQc—Pliocene–Pleistocene conglomerate. Q_1–Q_6 correspond to relative ages of alluvial surfaces; Q_6 is the oldest. The approximate location and orientation of the photograph are shown in Figure 1.

in low-angle fault contact against Mesozoic basement rocks that form the footwall of the Cañada David detachment. (2) Farther west toward the basin is Red Ridge, a prominent ridge of highly silicified and hydrothermally altered sandstone that is correlated with the Palm Spring Formation (Carter, 1977). Along its western margin, Red Ridge is bounded by a west-dipping normal fault that cuts all units except for the deposits associated with Q_7 and younger Quaternary alluvial fan surfaces that wrap around the Red Ridge and slope toward the Laguna Salada basin with an overall gradient of 2.26°. (3) Farther west, 1.5–2 km from the range-front fault, the broad Q_7 terrace is cut by a spectacular Quaternary scarp array that is 517 m wide and contains 11–13 individual scarps in any given transect (Fig. 3, profile 12). Many of these scarps predate the next youngest terrace (Q_6) and morphological analysis, based on scarp degradation, reveals that they are the oldest in the study area (Spelz et al., 2008). (4) The western limit of the prominent Q_7 terrace ends abruptly against a younger set of scarps that cuts Q_5 terraces. This younger set of surface ruptures is not completely exposed, but seems to be dominated by synthetic scarps that likely continue to the north. To the south, the younger scarps diverge from the array of older scarps that wraps around the southern end of Sierra El Mayor and follows the arcuate traces of the Cañada David detachment and Red Ridge faults (Fig. 11). Perhaps the most important aspect of the four distinct sets of faults and scarps along this structural transect is that they become systematically younger toward the basin, which clearly shows the progressive basinward migration of surface deformation.

Total net slip accommodated by scarps that make up the older array is 6.6 m, and although antithetic scarps are abundant, the ratio of horizontal:vertical net slip is only ~0.9, which corresponds to a steep hypothetical master-fault dip of 48° (Table 1). Due to the incomplete exposure and lack of correlatable surfaces across the younger scarps, they were not included in the reconstruction. However, because the younger scarps are found farther from the range front and are dominated by synthetic faults, they would likely increase the hypothetical master-fault dip.

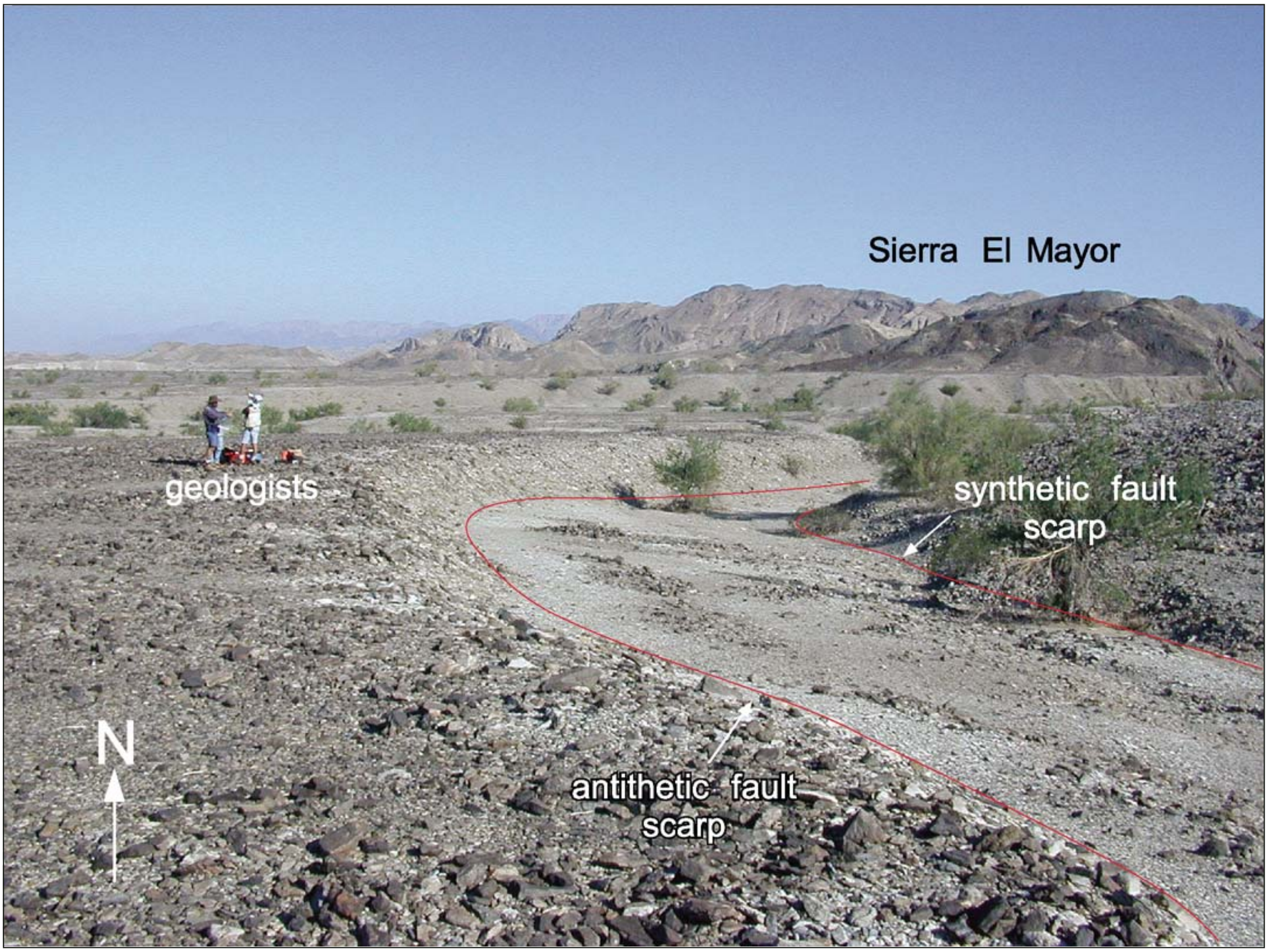

Figure 9. Field photograph of a strongly curvilinear mini-Quaternary graben cutting Q_5 deposits in the northern antiform domain. The approximate strike of the minigraben is subperpendicular to regional slope and modern drainages in this area. We propose that the corrugated morphology of the underlying master Cañada David detachment and the propagation of seismic slip into the thinning wedge of unconsolidated sediments are key factors influencing the dramatic change of orientation of the surface ruptures. See text for further discussion.

PATTERNS OF INTEGRATED SURFACE DEFORMATION

Integrated deformation across the scarp array shows marked along-strike variations (Table 1). The total slip varies by almost an order of magnitude, from 1.3 to 11.2 m. This pattern is to be expected because of gradients in the accumulation of late Quaternary slip and the fact that late Quaternary slip is heterogeneously preserved by the existing array of surface ruptures. However, it is more difficult to explain the equally remarkable variation in the ratio of horizontal:vertical net slip, which is reflected by the hypothetical dip of a master fault that ranges from 10° to the assumed inclination (65°) of the scarp-forming faults (Fig. 2; Table 1). The steeper hypothetical master-fault dips result from scarp arrays dominated by synthetic scarps, and, as antithetic scarps become more abundant and have greater offset, the hypothetical master-fault dip becomes shallower. Many factors, such as lithologic and mechanical heterogeneities, can affect the propagation of seismic ruptures, and it is unlikely that deformation is perfectly conserved when slip is transferred from a master fault to surface ruptures. Nonetheless, our data show strong correlations with different structural domains, which suggests that other factors control the ratio of horizontal:vertical net slip of the surface ruptures.

Important spatial variations in the scarp array can be seen by plotting hypothetical master-fault dip from different structural domains against distance from the range front (Fig. 12). This clearly shows that profiles in the northern antiform domain, which are closest to the range front, yield the lowest hypothetical master-fault dip, whereas profiles in the northern synform domain, which are farthest from the range front, yield the steepest hypothetical master-fault dip (Fig. 12). Profiles from the southern synform and southern antiform domains have intermediate values of both distance from the mountain front and hypothetical master-fault dip (Fig. 12). To explain this relationship we propose two hypotheses that need not be mutually

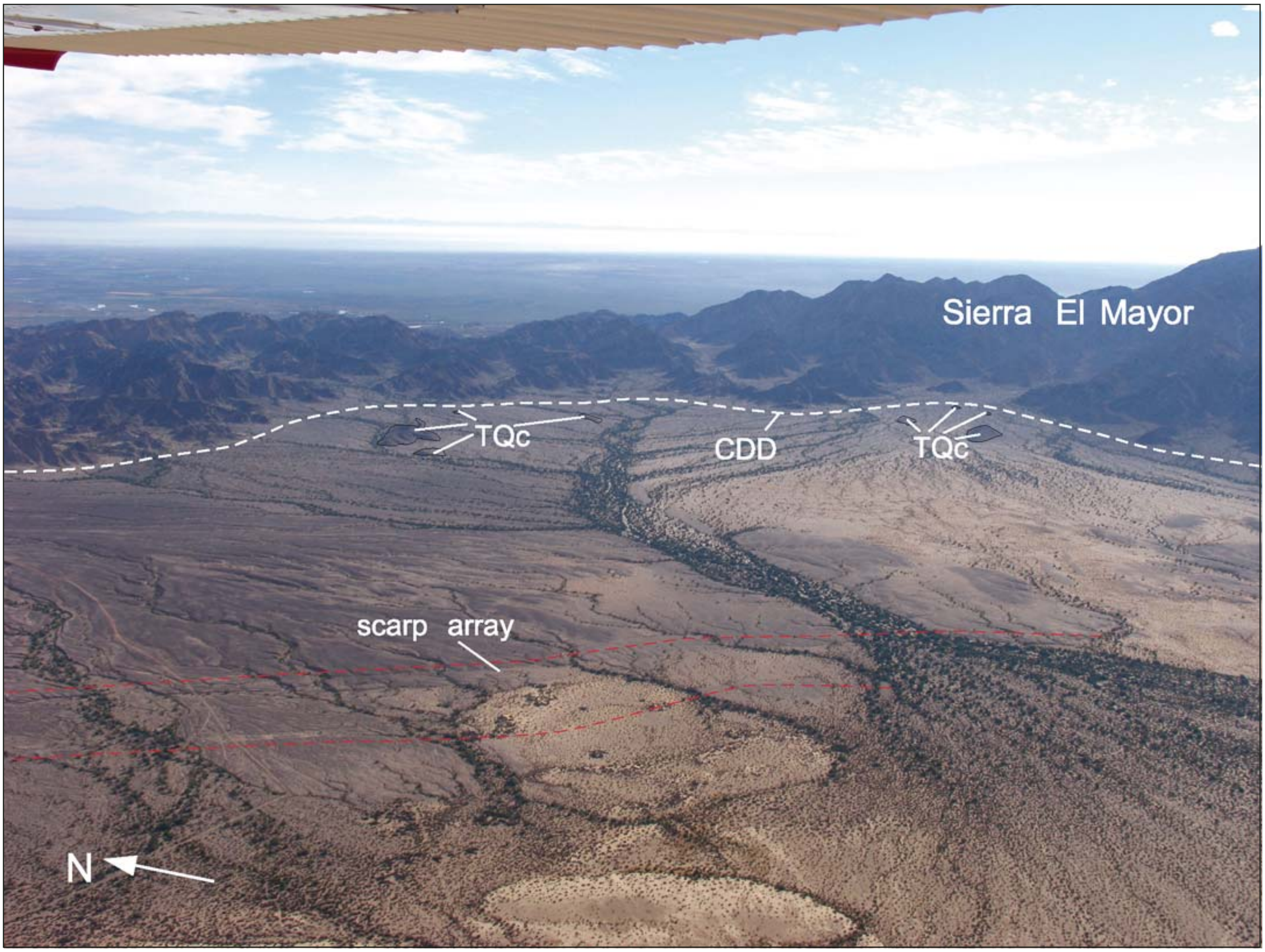

Figure 10. Oblique aerial photo of the southern synform domain showing the spatial separation of the late Quaternary scarp array and the trace of the Cañada David detachment (CDD). The CDD does not crop out in this domain, but its trace is reasonably well defined and must be between the mountain front and the outlying hills of Pliocene–Pleistocene conglomerate (TQc). The outer limits of the Quaternary scarp array are shown with red dashed lines. Note the straight traces of the individual scarps and the topographically subdued mountain front, which is in the process of being abandoned (see text for details). The strike length of the CDD visible in this photo is ~6.3 km. The approximate location and orientation of the photograph are shown in Figure 1.

exclusive and, as discussed in the following, are related to (1) propagation of seismic energy toward the surface, and (2) the subsurface geometry of the master fault.

Propagation of Seismic Slip

In this study we document the existence of an extensive Quaternary scarp array associated with a major low-angle normal fault that controls the eastern margin of the Laguna Salada basin. Although in rare cases it can be shown that seismic ruptures coincide with the exact trace of the master low-angle fault (e.g., Fig. 7), the vast majority are located west of the mountain front fault. Moreover, none of the scarp-forming faults is as shallowly dipping as the range-bounding detachment and most other faults are very high angle (~65°). Therefore, if seismogenic slip originated on a low-angle fault at depth, it must have been transferred to higher angle faults as it propagated to the surface.

The transfer of slip from a low-angle master fault to an array of multiple high-angle faults can explain many of the observed characteristics of the scarp array associated with the Cañada David detachment. For example, the fact that most scarps are found well west of the trace of the low-angle master fault (up to 14 km) would be expected if a pulse of seismogenic displacement propagates along the base of a thin wedge of weak unconsolidated sediments with no dominant preexisting faults. That is, as the overall thickness of the upper plate sediments decreases, its compaction and internal cohesion should also decrease. Near the surface, alluvial fan deposits are largely unconsolidated. Therefore, we propose that as seismic ruptures propagate toward the surface, it is likely that the sedimentary wedge could become weaker than the underlying master fault, which may cause seismic slip to become transferred to high-angle faults that propagate up into the wedge. It seems highly unlikely that the material in the shallowest portions of the sedimentary wedge is competent enough to allow seismic ruptures to propagate to the narrow limit of the wedge, which is

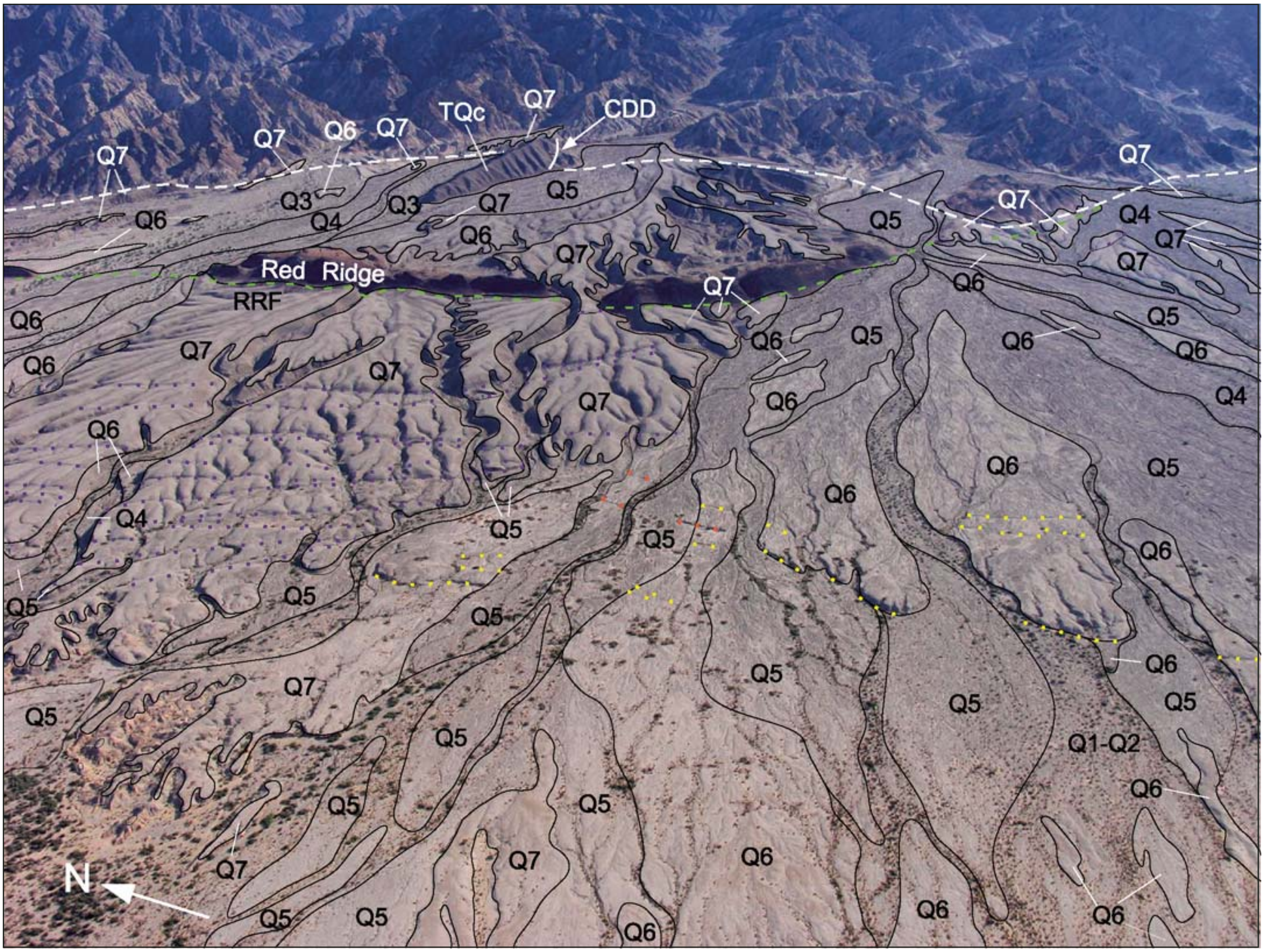

Figure 11. Oblique aerial photo of the southern limit of Sierra El Mayor showing four spatially distinct fault systems that become progressively younger toward the basin. The Cañada David detachment (CDD) and Red Ridge fault (RRF) are shown in white and green, respectively. Quaternary scarps that predate Q_6 are shown in purple, those that postdate Q_4 are shown in yellow, and those that cut Q_5 are shown in orange. See text for detailed description. Distance between the CDD and the farthest scarps is ~2.5 km. TQc—Pliocene–Pleistocene conglomerate. Q_1–Q_7 correspond to relative ages of alluvial surfaces; Q_7 is the oldest. The approximate location and orientation of the photograph are shown in Figure 1.

why scarps rarely are located along the trace of the master low-angle fault.

The transfer of slip to high-angle faults near the surface may also be affected by expected variations in other parameters that are thought to produce seismogenic slip on low-angle normal faults. For example, high pore-fluid pressure can cause failure on fault zones that are unfavorably oriented for slip like low-angle normal faults (Axen, 1992; Rice, 1992). However, in the seismogenic upper crust pore-fluid pressure decreases radically from lithostatic to hydrostatic pressures at depths of <2–5 km and becomes nil at the surface. Another factor that is called upon to produce failure on low-angle normal faults is the rotation of principal stress axes that will result if subhorizontal shear is applied to the base of the more rigid upper and middle crust (e.g., Yin, 1989; Wernicke, 1995; Westaway, 1999). However, this effect will diminish significantly with distance from the zone of subhorizontal shearing in the middle-lower crust and, moreover, an Andersonian stress configuration is required near the surface of the Earth, which must be a principal plane of stress. In summary, the transfer of slip to high-angle faults may also occur because both of the factors that are thought to cause slip on low-angle normal faults are negligible near the surface.

The great width of the scarp array, which reaches more than 500 m in the southern antiform domain, may also be explained by propagation of a seismic rupture along the base of a thinning wedge of variably consolidated sediments. Because the low-angle master fault defines the base of the sedimentary wedge in its hanging wall, it must also control other physical properties, such as the amount of compaction and cohesion of the material, that are largely dependent on the thickness. To the extent that the gradient in thickness is very low above a low-angle fault, it is unlikely for the wedge to contain abrupt thresholds in strength that would focus deformation into a narrow zone. Rather, rock failure should be distributed across a broad region with gradually varying strength properties. In addition, as the seismic rupture approaches the surface it must be traveling rapidly toward the trace of the range-bounding fault. This may cause the locus of surface deformation to follow slip propagation as surface ruptures begin to splay from the master fault, which would also help create a broad array of multiple scarps in a single seismic cycle.

The strongly curvilinear trace of many scarps may also be explained in part by the transfer of slip. The Cañada David detachment has a curvilinear trace defined by megamullions at many different scales, and in most cases the Quaternary scarps follow the small-scale deflections of the master fault. However, other scarps show radical along-strike variations that vary by ~60° in azimuth over distances of a few tens of meters, a geometry that we interpret to be more strongly related to the transfer of slip. Specifically, when slip is transferred from a well-defined fault plane into the overlying wedge, it must separate from the main structure that is controlling its propagation. If the rupture is not controlled by preexisting planar faults in the wedge, it may develop a more irregular expression with strongly curvilinear ruptures as well as multiple strands with lateral strain gradients.

Perhaps the most intriguing phenomenon of the scarp array that may be related to the transfer of seismic slip is the systematic increase in hypothetical dip of the master fault with distance from the trace of the range-front fault. If one assumes that the master fault projects into the subsurface at the same angle that it has at the surface (10°–20°), the integrated deformation of the surface ruptures should reflect seismic slip in terms of total offset and the ratio of horizontal and vertical components of the slip. The two most common ways of conserving the ratio of horizontal:vertical slip components during the transfer of slip from low-angle

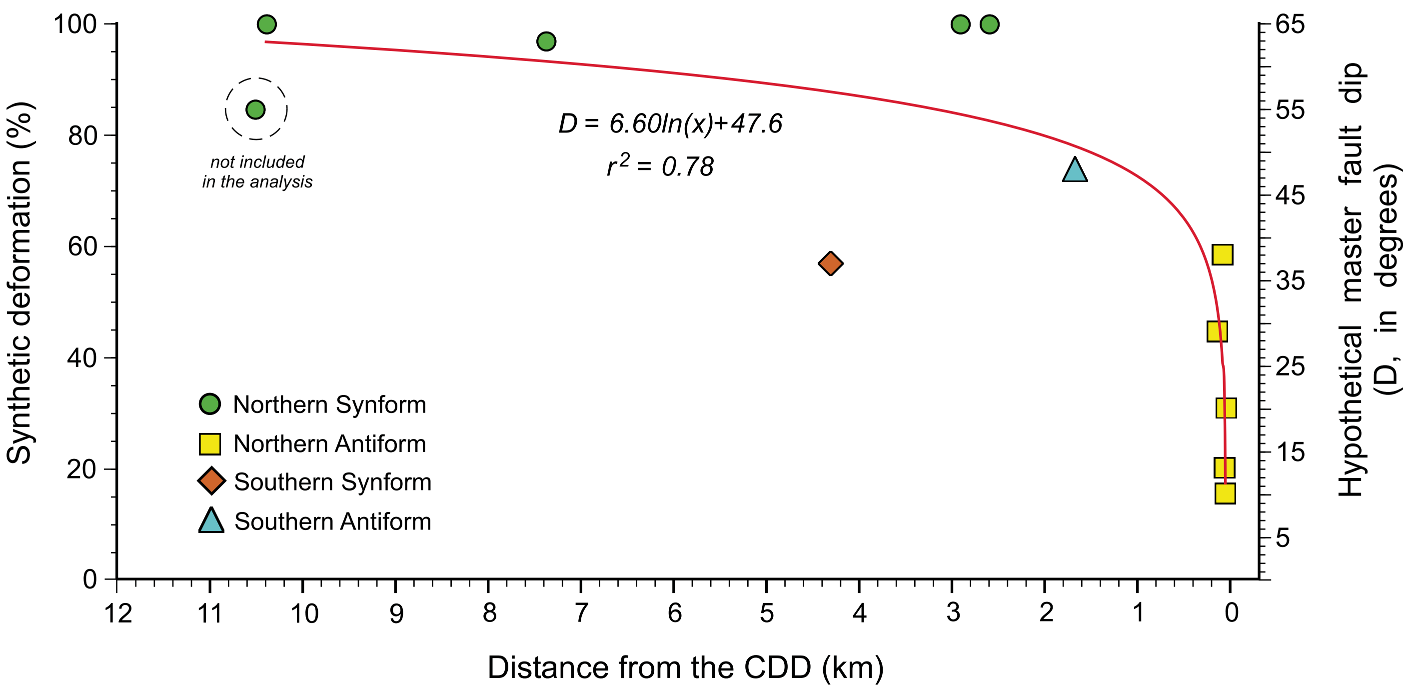

Figure 12. Variation of the master detachment dip (right axis) with distance from the range front. Left axis shows the percentage of deformation that is accommodated by synthetic surface ruptures across the scarp array. Scarp arrays located farther from the range front, where synthetic deformation is dominant, have steeper hypothetical dips of the master fault. The solid red line curve is the least-squares best-fit logarithmic function and shows the abrupt transition in hypothetical master-fault dip between 1 and 3 km from the mountain front. CDD—Cañada David detachment.

to high-angle normal faults is the formation of either a keystone graben or a rollover anticline (Fig. 13). A keystone graben is an array of two or more normal faults with at least one antithetic fault. The role of antithetic faults in the array is to simultaneously increase the integrated horizontal component and decrease the integrated vertical component of offset. Therefore, as the dip of the master fault decreases, the antithetic faults should increase in both number and offset relative to synthetic faults. The overall low hypothetical dip of the master fault when the scarp array is very close to the range-front fault indicates that keystone grabens are most likely to form when seismogenic rupture propagates to shallow levels of the sedimentary wedge. In contrast, a rollover anticline is a flexure in the hanging wall that accommodates a gradient in the vertical component of slip above a listric bend in the master fault. In western North America rollover anticlines are typically very broad features with half-wavelengths on a scale of tens of kilometers, and they are generally associated with normal faults with large

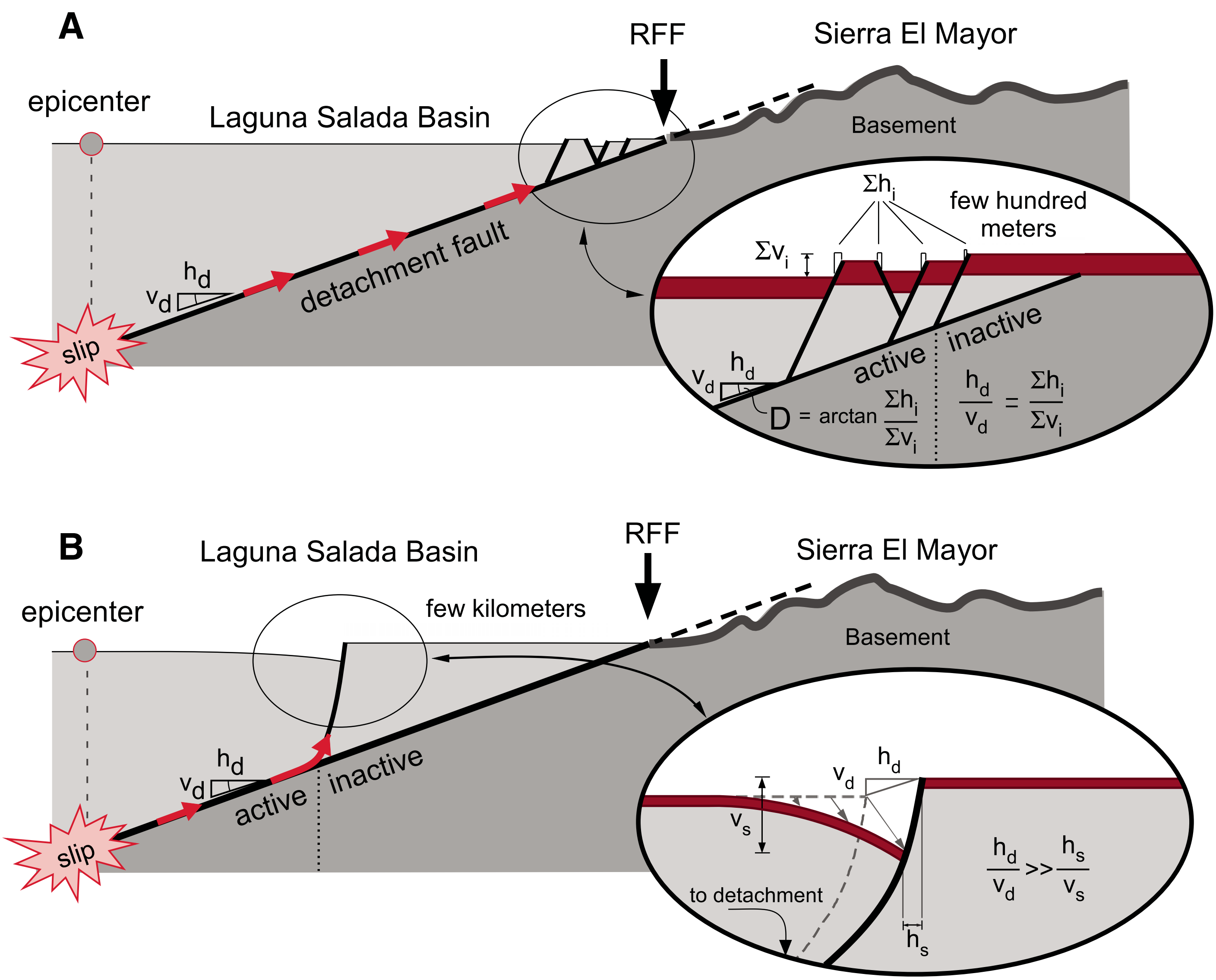

Figure 13. Schematic cross sections showing two mechanisms of transfer of seismogenic offset from a master low-angle normal fault to high-angle normal faults in the sedimentary wedge. The dominance of one mechanism or the other may be related to distance from the mountain front where the transfer occurs. (A) Keystone graben mechanism. Very close to the mountain front, the transfer of seismogenic slip produces one or more keystone grabens. The integrated horizontal (Σh_i) and vertical (Σv_i) components of shear across the scarp array are subequal to the horizontal (h_d) and vertical (v_d) components of seismogenic slip across the low-angle master fault, and thus the integrated deformation of the surface ruptures faithfully reproduces the dip (D) of the master fault. RFF—Range Front Fault. (B) Rollover anticline mechanism. Farther from the range front the transfer of seismogenic slip occurs deeper in the sedimentary wedge, inhibiting the formation of multiple scarps. In this case, a single synthetic scarp may form together with a subtle rollover anticline that results from penetrative deformation within the wedge. The shape of the anticline is greatly exaggerated in this schematic figure and was not detected in the topographic profiles of this study. For this mechanism, the ratio of horizontal to vertical deformation across the scarp array (h_s/v_s) does not faithfully reproduce the dip of the master detachment.

offset (>5 km). However, this does not mean that such a mechanism cannot accommodate the transfer of slip to a high-angle fault that has a small amount of total offset. The small offset would simply make it harder to recognize the broad flexure. Therefore, it is possible that subtle rollover anticlines may be associated with scarp array segments that yield large hypothetical dips of the master fault, and thus the integrated deformation of the surface ruptures alone would not accurately reflect the orientation of the master seismogenic fault at depth. If this is the case, our data show that such segments of the scarp array are found farther from the mountain front fault, and thus one would logically infer that the rollover-anticline mechanism would operate when the transfer of seismogenic slip to high-angle faults occurs deeper in the sedimentary wedge (Fig. 13).

Rolling-Hinge Hypothesis

Although nearly all of the important characteristics of surface deformation can be explained by assuming that the Cañada David detachment projects into the subsurface at a constant shallow angle, the simplest interpretation of our data is to infer that the master fault has an antilistric geometry and becomes steeper with distance from the mountain front; this may imply that it becomes steeper with depth in the shallow subsurface (Fig. 12). A master fault with an antilistric bend at shallow depths is actually the geometry predicted by the rolling-hinge model of detachment faulting, where the tectonically unloaded footwall rebounds isostatically to form an antiformal bulge that migrates in the direction of tectonic transport and essentially follows the displacement of the upper plate (e.g., Buck, 1988; Wernicke and Axen, 1988; Lavier et al., 1999). Deformational fabrics related to the rolling hinge were first reported by Bartley et al. (1989) and have been documented in large-magnitude normal fault systems throughout the world (see review by Axen and Bartley, 1997).

One aspect of the rolling-hinge model that has not been characterized by observational data is the actual geometry of the antilistric curve at the leading edge of the migrating antiform. Typically, folds related to isostatic rebound of the footwall are regional in scale with wavelengths similar to the across-strike dimension of the extended terranes (tens to hundreds of kilometers; e.g., Yin, 1991; Fletcher et al., 1995). In fact, the folds were originally modeled to form by flexural folding of continental crust with a finite elastic rigidity (Buck, 1988), which precludes the formation of folds with even moderate interlimb angles. However, the simplest interpretation of our data suggests that the master fault changes from dipping ~20° to ~65° within 1.5–5.0 km from the range-front fault, which suggest a much tighter bending of the master fault than is typically envisioned by the rolling-hinge model (Fig. 12).

In order to further evaluate the subsurface geometry of the Cañada David detachment we compiled seismicity data (from the catalog of the Seismic Network of Northwestern Mexico, RESNOM [Red Sísmica del Noroeste de México]), gravity data (Kelm, 1971; García-Abdeslem et al., 2001) and borehole logs (Martín-Barajas et al., 2001) for the Laguna Salada basin (Fig. 14). In the southern half of the basin, seismicity is mostly focused along the western margin, but there is also a distinct band of seismicity along the eastern margin. Both of these bands die out to the north and there is a significant seismic gap in the northern portion of the basin. The RESNOM network does not have any seismometers in the Laguna Salada basin, and thus seismicity with very low magnitude has been filtered out of the data set. Nonetheless, the seismic gap coincides extremely well with the extent of the 1892 surface rupture, which should have significantly relieved differential stress in this segment (Fig. 14). This relationship strongly suggests that seismicity along both the western and eastern margins of the Laguna Salada basin is related to the main basin-controlling faults along the eastern margin.

Figure 14 shows contours of the Bouguer gravity anomaly that were derived from an extensive data set collected by Kelm (1971) and García-Abdeslem et al. (2001). The most notable feature is the major gravity gradient along the eastern margin of the Laguna Salada basin, which Kelm (1971) named the eastern side anomaly. In the north, the 20 mgal gradient coincides with the trace of the high-angle Laguna Salada fault, and here García-Abdeslem et al. (2001) modeled the lower density basin fill to extend to 3.5 km depth. However, toward the south, adjacent to the low-angle Cañada David detachment, the gravity anomaly increases to 40 mgal with a gradient comparable to farther north. This key observation is consistent with the abrupt change in master-fault geometry that was inferred from the scarp array data.

A series of east-west cross sections shows our preferred interpretation of the subsurface structural geometry of the Laguna Salada basin (Fig. 15). Both the borehole and gravity data are consistent with the overall geometry of an asymmetric half-graben basin with the main basin-controlling faults on the eastern margin. Although detailed modeling of the gravity data is beyond the scope of this study, we infer that the location of the eastern side anomaly defined by Kelm (1971) should coincide with large relief across the fault-controlled margin of the sedimentary fill. Because the magnitude of the gravity gradient increases to the south, it is safe to infer that the relief across the eastern margin should also increase toward the south. This strongly suggests that the low-angle Cañada David detachment bends into a much higher angle orientation in the shallow subsurface along the eastern margin of the basin, consistent with the simplest interpretation of the fault scarp data (Fig. 12). Another factor that can contribute significantly to the 40 mgal gravity anomaly is the juxtaposition of upper plate basement with lower plate basement across a steep ramp in the master fault, which we propose to project downward through most of the seismogenic upper crust (Fig. 15). Although none of the data presented in this study helps to define the geometry of the master fault at the deepest levels of the cross sections, we speculate that the ramp becomes shallow again near the brittle-ductile transition (~15 km depth); this is consistent with previous versions of the rolling-hinge model (e.g., Buck, 1988; Wernicke and Axen, 1988).

Seismicity within 6 km of each profile was projected onto the cross sections and demonstrates well the southward increase in seismic activity (Fig. 15). The closest seismic station in the RESNOM network is found ~10 km east of Laguna Salada in the Mexicali valley, and thus hypocenter depth is not well determined. Nonetheless, most of the hypocenters are at depths of 2–17 km, consistent with the microseismicity recorded by the temporary local network used by García-Abdeslem et al. (2001), which recorded more accurate hypocenter locations in the Laguna Salada basin. The inferred geometry of the Cañada David detachment seems to coincide well with the distribution of seismicity along the eastern margin of the basin, and significant seismicity is also associated with antithetic faults along the western margin of the basin. The relative magnitude of finite slip across these two fault systems is illustrated in Figure 15C. The major erosional unconformity that forms the flat surface of the high Sierra Juarez can be tracked across the western antithetic fault array, which accommodates <2 km of total offset. In contrast, the same unconformity is exposed in Sierra El Mayor and is offset by ~15 km across the Cañada David detachment. This is actually a minimum estimate because the fault bifurcates in this section, and an additional amount of slip (probably several kilometers) is accommodated by the structurally lower strand.

The distribution of surficial lacustrine sediments that mark the modern depocenter of the Laguna Salada basin also can be used to help define the subsurface geometry of the Cañada David detachment. After drawing the antilistric

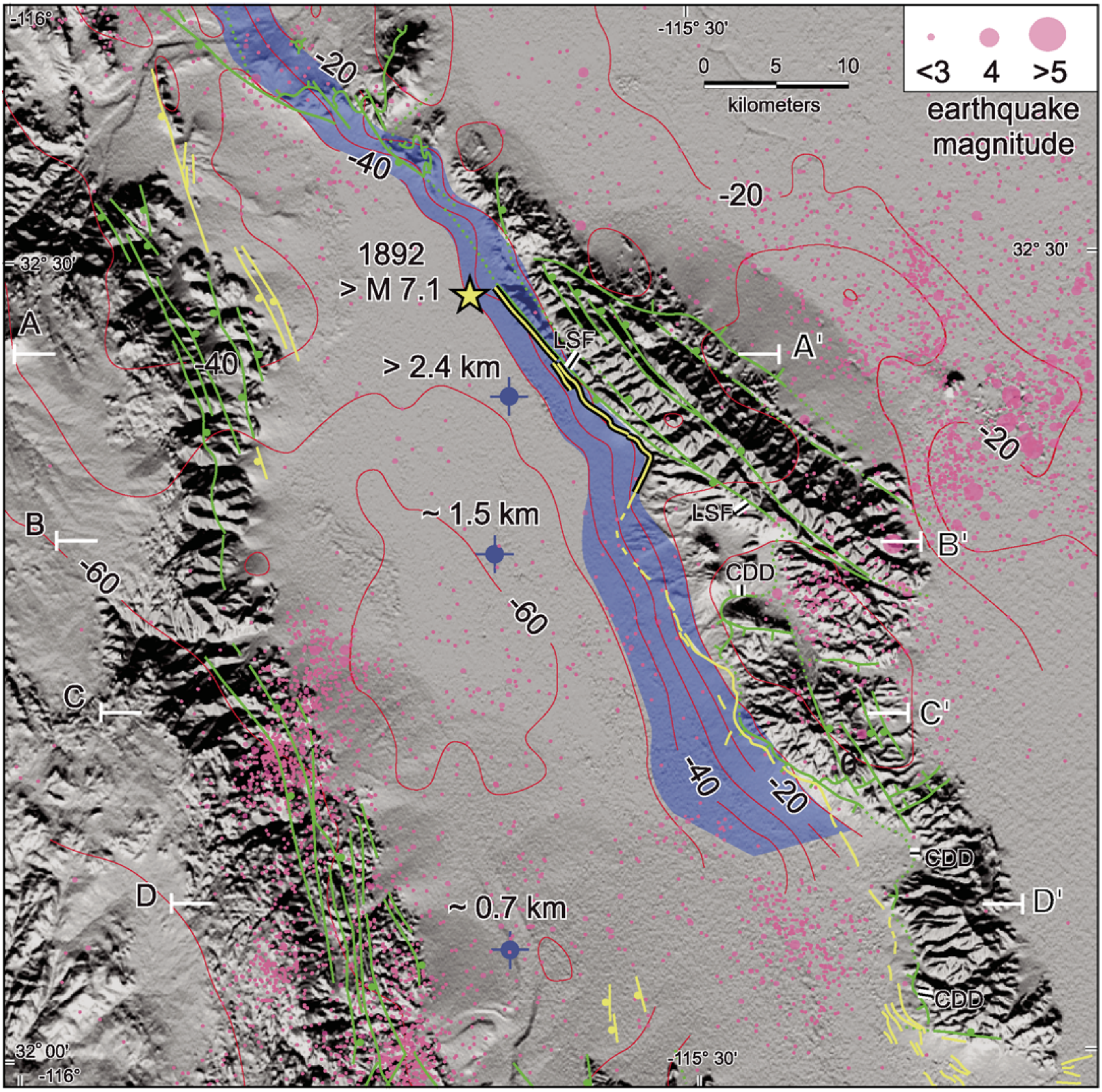

Figure 14. Shaded relief map of the Laguna Salada basin showing distribution of faults, Quaternary scarps, seismicity, contoured Bouguer gravity anomaly (contour interval = 10 mgal), and boreholes. A prominent seismic shadow is observed adjacent to the 1892 rupture in the northern Laguna Salada basin. A major gravity anomaly (shaded blue) is associated with both the high-angle Laguna Salada fault (LSF) and the low-angle Cañada David detachment (CDD). This is the "eastern side anomaly" first described by Kelm (1971). Digital elevation model (DEM) data were compiled from Shuttle Radar Topography Mission (SRTM) and GEoModelos De Elevación (GEMA) data sets. Seismic data were compiled from the catalog of the Seismic Network of Northwestern Mexico (RESNOM; Red Sísmica del Noroeste de México) and include data from January 1983 to December 2006. Contours of the Bouguer gravity anomaly were obtained from García-Abdeslem et al. (2001). Borehole data were reported by Martín-Barajas et al. (2001). The locations for the four serial cross sections (A-A', B-B', C-C', and D-D') correspond to those shown in Figure 15.

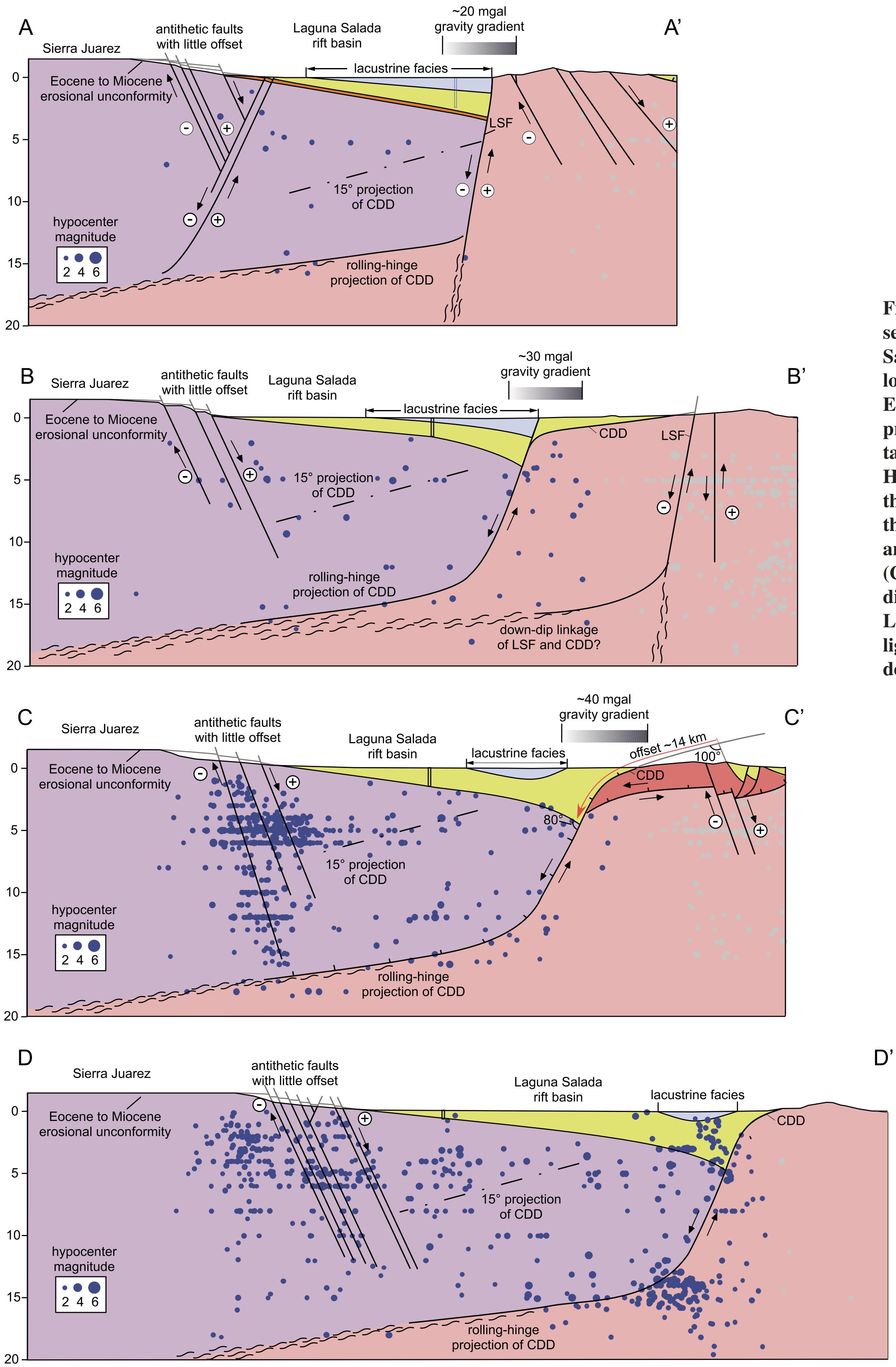

Figure 15. Serial geologic cross sections across the Laguna Salada basin. Section lines are located in Figures 1 and 14. Earthquake hypocenters were projected from a maximum distance of 6 km from each profile. Hypocenters of earthquakes that plot east of the trace of the Laguna Salada fault (LSF) and Cañada David detachment (CDD) are not considered to be directly related to faults in the Laguna Salada basin and are light gray. See text for further description.

geometry to be consistent with the gravity, borehole, and seismic data, the result is that in each cross section the surficial lacustrine sediments directly overlie the steep ramp of the master fault. Therefore, the depocenter of the basin coincides well with the portion of the master fault that should produce the most vertical subsidence.

To briefly address the alternative hypothetical geometry of the Cañada David detachment, its projection from the surface trace is shown in each cross section assuming a constant 15° inclination (Fig. 15). Although a fault with such geometry seems to coincide with a weaker and more diffuse band of shallow seismicity, it would be difficult to explain the origin of the deeper seismicity along the eastern margin if this were the true geometry of the master fault (Figs. 15C, 15D). In addition, it would be very difficult to explain the eastern margin gravity gradient and location of the depocenter within the framework of this alternative geometry.

Another alternative hypothesis that is more consistent with the gravity, seismic, and borehole data is to consider two fault systems: a younger high-angle fault that cuts an older low-angle fault. In fact, this configuration applies well to the northern synform domain, where a major segment of the range-bounding detachment has been abandoned and the active scarp array is dominated by synthetic ruptures that yield hypothetical master-fault dips of 65°. However, in the northern antiform domain, scarps have propagated all the way to the surface trace of the detachment. This demonstrates that major segments of the low-angle range-bounding fault are still active, which certainly would not be expected if they were crosscut by a major high-angle fault. In addition, it makes very little sense for any fault to only accommodate subsidence and not have an equally important component of uplift. The steep fault segments shown in the sections of Figure 15 accommodate several kilometers of syntectonic sedimentation. However, in several sections the only surface expression of uplift is associated with the trace of the range-bounding low-angle normal fault, which does not directly overlie the steeper fault segments (Figs. 15C, 15D). These relationships preclude two temporally distinct faults and instead require a single fault with a shallow antilistric bend.

In summary, we strongly favor a master fault with a shallow antilistric geometry. As inferred from the fault-scarp data, we propose that the change in inclination of the master fault is not a smooth flexure, but instead is much more abrupt than originally thought. The location of Quaternary scarps near the trace of the Cañada David detachment (e.g., northern antiform domain) indicates that seismogenic ruptures may propagate through this inferred abrupt change in geometry in the shallow subsurface.

BASINWARD MIGRATION OF NORMAL FAULTING

The progressive basinward migration of faulting is implicit to the rolling-hinge model of the evolution of large-magnitude normal faults. Isostatic rebound of the footwall causes the master fault to rotate to a low-angle geometry. Almost all core complexes contain segments of the master fault that have been rotated through horizontal and form the back-dipping limbs of footwall antiforms. The back-dipping segments of the master fault show an apparent thrust sense of shear, but stranded klippes of the upper plate consistently display the omission of crustal section across the fault, which is a defining characteristic of normal faults. It is thought that upon rotation, the shallowly dipping fault segments are abandoned, and deformation migrates in the direction of tectonic transport as new high-angle faults form in the trailing portion of the hanging wall (e.g., Buck, 1988; Wernicke and Axen, 1988). As illustrated by Wernicke and Axen (1988), this basinward migration occurs in steps that are equivalent to the width (generally several kilometers) of hanging-wall fault blocks. However, the visualization of the rolling-hinge model is restricted to two-dimensional profiles drawn parallel to tectonic transport. Field relationships derived in this study provide new insight for the three dimensional patterns of basinward migration of deformation during the evolution of a major low-angle normal fault.

As we have proposed, the late Quaternary scarp array along most of the eastern margin of the Laguna Salada basin can be interpreted to represent the latest phase of slip across the Cañada David detachment. As a rule, the late Quaternary scarp array does not coincide exactly with the master fault trace, but rather is consistently found a finite distance toward the basin (Table 1). Therefore, the entire scarp array, which extends 55–60 km along strike, can be considered to represent the basinward migration of the most recent phase of slip across the master fault.

Map relationships clearly show that the most profound basinward migration of deformation is consistently associated with the macroscopic synform domains where the scarp array diverges dramatically from the trace of the Cañada David detachment (Figs. 1, 2, and 14). In the northern synform domain the scarp array extends south from the Laguna Salada fault in a manner that is geometrically and kinematically similar to the intersection of the Cañada David detachment and Laguna Salada fault found ~10 km to the east. A new mountain front is clearly forming where the active faults have already significantly uplifted a major tectonic block and exposed even some of the oldest basin fill to erosion. As mentioned previously, faults that control Cerro Colorado must have been active before the onset of faulting along the new mountain front defined by the Cañón Rojo and Chupamirtos faults (Figs. 1 and 2). However, the fact that Cerro Colorado is composed entirely of basin-fill strata requires that the associated faulting and uplift significantly postdated the onset of faulting along the Cañada David detachment. Therefore, we propose that the locus of deformation migrated in two major steps from the long-lived mountain front defined by the trace of the Cañada David detachment. The new tectonic block in the northern synform domain is more than 10 km in width, but it does not extend laterally along the entire length of the Cañada David detachment, as might be expected from the two-dimensional profiles that depict the rolling-hinge model. Instead, the block rapidly pinches out to the south as the scarp array closely approaches the trace of the Cañada David detachment in the northern antiform domain.

The scarp array also diverges from the trace of the Cañada David detachment in the southern synform domain, where another new, lozenge-shaped, tectonic block with a width of ~4 km has formed. This new mountain front is in an incipient stage of formation and significant dissection of the basin fill in its footwall has not yet started (Fig. 10).

In the southern antiform domain, the scarp array generally is within 1–2 km of the trace of the Cañada David detachment. As described earlier, in this domain we recognize four distinct generations of Quaternary faults that show a progressive basinward migration of deformation, but in much smaller steps (<1 km) than observed in the two macroscopic synformal domains.

In summary, new tectonic blocks have clearly formed in the hanging wall of the Cañada David detachment, but they are not continuous along strike. Instead they are largely restricted to macroscopic synformal domains, where they form lozenge-shaped blocks that pinch out toward the macroscopic antiformal domains. Therefore, we infer that the basinward migration of deformation largely occurs in synformal megamullion domains, driven perhaps by the reorganization of the fault to adopt a more mechanically favorable geometry with less surface area. The fact that very low angle segments of the Cañada David detachment are still clearly active in the northern antiform domain may give a measure of how much back rotation the master fault can undergo before it becomes abandoned in favor of higher-angle faults in the basin.

CONCLUSIONS

The Cañada David detachment is a low-angle normal fault that can be mapped as a single structure along the 55–60-km-long mountain front of the western margin of Sierra El Mayor. It cuts Miocene–Pleistocene strata and is inferred to have accommodated 5–7 km of denudation since ca. 12 Ma ago (Axen et al., 2000). An extensive array of late Quaternary surface ruptures exists along the entire length of the Cañada David detachment. This study confirms the hypothesis that the Cañada David detachment is active and the scarp array represents its latest phase of motion. We identify four key relationships that can be more widely used to identify and give new insight into the evolution of active low-angle normal faults.

1. There is a strong spatial coincidence between the lateral extent of the Cañada David detachment and the late Quaternary scarp array. The northern limit of the scarp array ends abruptly against the Laguna Salada fault in exactly the same manner as the northern limit of the Cañada David detachment. In the south, the Quaternary scarp array wraps around the southwestern margin of Sierra El Mayor, becomes diffuse, and ruptures disappear within a few kilometers of the southernmost exposures of the Cañada David detachment.

2. The scarp-forming faults do not crosscut the entire width of the fault zone of the Cañada David detachment, but instead seem to merge with cataclastic fabrics of the Cañada David detachment. In certain segments, like the northern antiformal domain, scarps show radical changes in along-strike orientation and closely follow the smaller scale megamullion corrugations in the Cañada David detachment.

3. At the macroscopic scale, the scarp array extends across synformal megamullions and forms structural bridges that connect antiformal megamullions where the array more closely follows the trace of the Cañada David detachment. This basinward migration of deformation mainly occurs in macroscopic synformal domains where large segments of the Cañada David detachment have been abandoned and lozenge-shaped tectonic blocks have been transferred from the hanging wall to the footwall.

4. Antithetic scarps are abundant in the scarp array, and they significantly increase the ratio of horizontal extension compared to vertical uplift of the mountain range, which is expected if surface ruptures are controlled by slip on a low-angle normal fault. However, the ratio of horizontal:vertical slip across the scarp array abruptly decreases with distance from the mountain front, and beyond 2–4 km, the array is dominated by high-angle synthetic scarps. This likely reflects either a change in mechanism of accommodation of horizontal deformation (keystone grabens versus rollover anticlines) or a shallow antilistric geometry of the master range-bounding fault, similar to the predicted geometry of large-offset normal faults in the rolling-hinge model. These two hypotheses need not be mutually exclusive, and independent observations from the Laguna Salada basin strongly suggest that the Cañada David detachment has an abrupt antilistric geometry in the shallow subsurface.

ACKNOWLEDGMENTS

This paper benefited greatly from discussions with numerous colleagues working in Laguna Salada, including Lewis Owen, Arturo Martin-Barajas, Jose Frez, Francisco Suarez-Vidal, Gary Axen, Juan-Manuel Espinoza, Luis Munguia, and many others. We are grateful for careful and insightful reviews from Terry Pavlis, Ramon Arrowsmith, and an anonymous reviewer. The work was financially supported by CONACYT (Consejo Nacional de Ciencia y Tecnología) grant 81463, a grant from the U.S. National Science Foundation Margins program, as well as internal funding from CICESE (Centro de Investigación Científica y de Educación Superior de Ensenada).

REFERENCES CITED

Abbott, R.E., Louie, J.N., Caskey, S.J., and Pullammanappallil, S., 2001, Geophysical confirmation of low-angle normal slip on the historically active Dixie Valley fault, Nevada: Journal of Geophysical Research, v. 106, p. 4169–4181, doi: 10.1029/2000JB900385.

Abers, G.A., 1991, Possible seismogenic shallow-dipping normal faults in the Woodlark-D'Entrecasteaux extensional province, Papua New Guinea: Geology, v. 19, p. 1205–1208, doi: 10.1130/0091-7613(1991)019<1205:PSSDNF>2.3.CO;2.

Axen, G.J., 1992, Pore pressure, stress increase, and fault weakening in low-angle normal faulting: Journal of Geophysical Research, v. 97, no. B6, p. 8979–8991, doi: 10.1029/92JB00517.

Axen, G.J., 2004, Mechanics of low-angle normal faults, *in* Karner, G.D., et al., eds., Rheology and deformation of the lithosphere at continental margins: New York, Columbia University Press, p. 46–91.

Axen, G.J., and Bartley, J.M., 1997, Field tests of rolling hinges: Existence, mechanical types, and implications for extensional tectonics: Journal of Geophysical Research, v. 102, p. 20,515–20,537, doi: 10.1029/97JB01355.

Axen, G.J., and Fletcher, J.M., 1998, Late Miocene–Pleistocene extensional faulting, northern Gulf of California, Mexico and Salton Trough, California: International Geology Review, v. 40, p. 217–244.

Axen, G.J., Fletcher, J.M., Cowgill, E., Murphy, M., Kapp, P., MacMillan, I., Ramos-Velazquez, E., and Aranda-Gomez, J., 1999, Range-front fault scarps of the Sierra El Mayor, Baja California: Formed above a low-angle normal fault?: Geology, v. 27, p. 247–250, doi: 10.1130/0091-7613(1999)027<0247:RFFSOT>2.3.CO;2.

Axen, G.J., Grove, M., Stockli, D., Lovera, O.M., Rothstein, D.A., Fletcher, J.M., Farley, K., and Abbott, P.L., 2000, Thermal evolution of Monte Blanco dome: Low-angle normal faulting during Gulf of California rifting and late Eocene denudation of the eastern Peninsular Ranges: Tectonics, v. 19, p. 197–212, doi: 10.129/1999TC001123.

Barnard, F.L., 1968, Structural geology of the Sierra de los Cucapas, northeastern Baja California, Mexico, and Imperial County, California [Ph.D. thesis]: Boulder, University of Colorado, 157 p.

Bartley, J.M., Fletcher, J.M., and Glazner, A.F., 1989, Tertiary extension and contraction of lower plate rocks in the Central Mojave Metamorphic Core Complex: Implications for footwall uplift processes in continental extension: Geological Society of America Abstracts with Programs, v. 21, no. 6, p. A25.

Boncio, P., Brozzetti, F., and Lavecchia, G., 2000, Architecture and seismotectonics of a regional low-angle normal fault zone in central Italy: Tectonics, v. 19, p. 1038–1055, doi: 10.1029/2000TC900023.

Brady, R., Wernicke, B., and Fryxell, J., 2000, Kinematic evolution of a large-offset continental normal fault system, South Virgin Mountains, Nevada: Geological Society of America Bulletin, v. 112, p. 1375–1397.

Buck, R., 1988, Flexural rotation of normal faults: Tectonics, v. 7, p. 959–973, doi: 10.1029/TC007i005p00959.

Carter, D.L., 1977, Late Quaternary erosional and depositional history of Sierra del Mayor, Baja California, Mexico [Ph.D. thesis]: Los Angeles, University of Southern California, 262 p.

Chiaraluce, L., Piccinini, D., Collettini, C., and Chiarabba, C., 2006, Microseismic activity on a low angle normal fault (northern Apennines, Italy): Geophysical Research Abstracts, v. 8, no. 08035.

Chora-Salvador, J.M., 2003, Analisis cinematico de fallas neogenicas normales de alto y bajo angulo en la Sierra Cucapa, Baja California, Mexico [Masters thesis]: Centro de Investigacion Cientifica y de Educacion Superior de Ensenada (CICESE), 107 p.

Cichanski, M., 2000, Low-angle, range-flank faults in the Panamint, Inyo, and Slate ranges, California: Implications for recent tectonics of the Death Valley region: Geological Society of America Bulletin, v. 112, p. 871–883, doi: 10.1130/0016-7606(2000)112<0871:LARFFI>2.3.CO;2.

Collettini, C., and Sibson, R.H., 2001, Normal faults, normal friction?: Geology, v. 29, p. 927–930, doi: 10.1130/0091-7613(2001)029<0927:NFNF>2.0.CO;2.

Dorsey, R., and Martín-Barajas, A., 1999, Sedimentation and deformation in a Pliocene-Pleistocene transtensional supradetachment basin, Laguna Salada, northwest Mexico: Basin Research, v. 11, p. 205–221, doi: 10.1046/j.1365-2117.1999.00096.x.

Doser, D.I., 1994, Contrasts between source parameters of M≥5.5 earthquakes in northern Baja California and southern California: Geophysical Journal International, v. 116, p. 605–617.

Fletcher, J.M., Bartley, J.M., Martin, M.W., Glazner, A.F., and Walker, J.D., 1995, Large-magnitude continental extension: An example from the central Mojave metamorphic core complex: Geological Society of America Bulletin, v. 107, p. 1468–1483, doi: 10.1130/0016-7606(1995)107<1468:LMCEAE>2.3.CO;2.

Floyd, J.S., Mutter, J.C., Goodliffe, A.M., and Taylor, B., 2001, Evidence for fault weakness and fluid flow within an active low-angle normal fault: Nature, v. 411, p. 779–783, doi: 10.1038/35081040.

García-Abdeslem, J., Espinosa-Cardena, J.M., Munguía-Orozco, L., Wong-Ortega, V.M., and Ramírez-Hernández, J., 2001, Crustal structure from 2-D gravity and magnetic data modeling, magnetic power spectrum inversion, and seismotectonics in the Laguna Salada basin, northern Baja California, Mexico: Geofísica Internacional, v. 40, no. 2, p. 67–85.

Hatzfeld, D., Karakostas, V., Ziazia, M., Kassaras, I., Papadimitriou, E., Makropoulos, K., Voulgaris, N., and Papaioannou, C., 2000, Microseismicity and faulting geometry in the Gulf of Corinth (Greece): Geophysical Journal International, v. 141, p. 438–456, doi: 10.1046/j.1365-246x.2000.00092.x.

Hayman, N.W., Knott, J.R., Cowan, D.S., Nemser, E., and Sarna-Wojcicki, A.M., 2003, Quaternary low-angle slip on detachment faults in Death Valley, California: Geology, v. 31, p. 343–346, doi: 10.1130/0091-7613(2003)031<0343:QLASOD>2.0.CO;2.

Jackson, J.A., 1987, Active normal faulting and crustal extension, *in* Coward, M.P., et al., eds., Continental extensional tectonics: Geological Society of London Special Publication 28, p. 3–17.

Kelm, L.D., 1971, A gravity and magnetic study of the Laguna Salada area, Baja California, Mexico [M.S. thesis]: San Diego, California, San Diego State College, 103 p.

Lavier, L.L., Buck, W.R., and Pollakov, A.N.B., 1999, Self-consistent rolling-hinge model for the evolution of large-offset low-angle normal faults: Geology, v. 27, p. 1127–1130, doi: 10.1130/0091-7613(1999)027<1127:SCRHMF>2.3.CO;2.

Leeds, A., 1979, The locations of the 1954 northern Baja California earthquake: San Diego, University of California, 101 p.

Little, T.A., Monteleone, B., Baldwin, S.L., and Fitzgerald, P.G., 2006, Rapid slip-rate and low shear strength of a high finite-slip low-angle normal fault: Normanby Island, Woodlark Rift, Papua New Guinea: Eos (Transactions, American Geophysical Union), v. 87, Fall Meeting Supplement, abs. #T53A–1572.

Martín-Barajas, A., Vázquez-Hernández, S., Carreño, A.L., Helenes, J., Suárez-Vidal, F., and Álvarez-Rosales, J., 2001, Late Neogene stratigraphy and tectonic control on facies evolution in the Laguna Salada Basin, northern Baja California, Mexico: Sedimentary Geology, v. 144, p. 5–35, doi: 10.1016/S0037-0738(01)00133-6.

Miller, E.L., Gans, P.B., and Garing, J., 1983, The Snake Range Décollement: An exhumed mid-Tertiary brittle-ductile transition: Tectonics, v. 2, p. 239–263, doi: 10.1029/TC002i003p00239.

Miller, M.B., and Pavlis, T.L., 2005, The Black Mountains turtlebacks; Rosetta stones of Death Valley tectonics: Earth-Science Reviews, v. 73, p. 115–138, doi: 10.1016/j.earscirev.2005.04.007.

Mueller, K.J., and Rockwell, T.K., 1995, Late Quaternary activity of the Laguna Salada fault in northern Baja California, Mexico: Geological Society of America Bulletin, v. 107, p. 8–18, doi: 10.1130/0016-7606(1995)107<0008:LQAOTL>2.3.CO;2.

Numelin, T., Kirby, E., Walker, J.D., and Didericksen, B., 2007, Late Pleistocene slip on a low-angle normal fault, Searles Valley, California: Geosphere, v. 3, no. 3, p. 163–176.

Proffett, J.M., Jr., 1977, Cenozoic geology of the Yerington district, Nevada, and implications for the nature and origin of Basin and Range faulting: Geological Society of America Bulletin, v. 88, p. 247–266, doi: 10.1130/0016-7606(1977)88<247:CGOTYD>2.0.CO;2.

Rice, J.R., 1992, Fault stress states, pore pressure distributions, and the weakness of the San Andreas fault, *in* Evans, B., and Wong, T. F., eds., Fault mechanics and transport properties of rock: A Festchrift in honor of W.F. Brace: San Diego, California, Academic Press, p. 475–503.

Rietbrock, A., Tiberi, C., Scherbaum, F., and Lyon-Caen, H., 1996, Seismic slip on a low angle normal fault in the Gulf of Corinth evidence from high-resolution cluster analysis of microearthquakes: Geophysical Research Letters, v. 23, p. 1817–1820, doi: 10.1029/96GL01257.

Siem, M., and Gastil, G., 1994, Mid-Tertiary to Holocene extension association with the development of the Sierra El Mayor Metamorphic Core Complex, northeastern Baja California, Mexico, *in* McGill, S.F., and Ross, T.M., eds., Geological investigations of an active margin: Geological Society of America Cordilleran Section Meeting Guidebook: Redlands, California, San Bernardino County Museum Association, p. 107–119.

Sorel, D., 2000, A Pleistocene and still-active detachment fault and the origin of the Corinth-Patras rift, Greece: Geology, v. 28, p. 83–86, doi: 10.1130/0091-7613(2000)28<83:APASDF>2.0.CO;2.

Spelz, R.M., Fletcher, J.M., Owen, L.A., and Caffee, M.W., 2008, Quaternary alluvial-fan development, climate and morphologic dating of fault scarps in Laguna Salada, Baja California, Mexico: Geomorphology, v. 102, p. 578–594, doi: 10.1016/j.geomorph.2008.06.001.

Stewart, J.H., 1998, Regional characteristics, tilt domains, and extensional history of the later Cenozoic Basin and Range Province, western North America, *in* Faulds, J. E., and Stewart, J.H., eds., Accommodation zones and transfer zones; The regional segmentation of the Basin and Range Province: Geological Society of America Special Paper 323, p. 47–74.

Taylor, M., Kapp, P., Stockli, D., Lee, J., and Lin, D., 2006, The Longgur-Shan Detachment System, west central Tibet: An example of an active low-angle normal fault?: Eos (Transactions, American Geophysical Union), v. 87, Fall Meeting Supplement, abs. #T31B–0446.

Wernicke, B., 1995, Low-angle normal faults and seismicity: A review: Journal of Geophysical Research, v. 100, no. B10, p. 20,159–20,174, doi: 10.1029/95JB01911.

Wernicke, B., and Axen, G.J., 1988, On the role of isostasy in the evolution of normal fault systems: Geology, v. 16, p. 848–851, doi: 10.1130/0091-7613(1988)016<0848:OTROII>2.3.CO;2.

Westaway, R., 1999, The mechanical feasibility of low-angle normal faulting: Tectonophysics, v. 308, p. 407–443, doi: 10.1016/S0040-1951(99)00148-1.

Yin, A., 1989, Origin of regional, rooted low-angle normal faults; a mechanical model and its tectonic implications: Tectonics, v. 8, p. 469–482, doi: 10.1029/TC008i003p00469.

Yin, A., 1991, Mechanisms for the formation of domal and basinal detachment faults: A three-dimensional analysis: Journal of Geophysical Research, v. 96, no. B9, p. 14,577–14,594, doi: 10.1029/91JB01113.

Manuscript Received 29 August 2008
Revised Manuscript Received 5 February 2009
Manuscript Accepted 8 March 2009